

Hamiltonian Hopf bifurcations in the discrete nonlinear Schrödinger trimer: oscillatory instabilities, quasiperiodic solutions and a 'new' type of self-trapping transition

Magnus Johansson

Department of Physics and Measurement Technology, Linköping University, S-581 83 Linköping, Sweden

E-mail: mjn@ifm.liu.se

Abstract. Oscillatory instabilities in Hamiltonian anharmonic lattices are known to appear through Hamiltonian Hopf bifurcations of certain time-periodic solutions of multibreather type. Here, we analyze the basic mechanisms for this scenario by considering the simplest possible model system of this kind where they appear: the three-site discrete nonlinear Schrödinger model with periodic boundary conditions. The stationary solution having equal amplitude and opposite phases on two sites and zero amplitude on the third is known to be unstable for an interval of intermediate amplitudes. We analyze the nature of the two bifurcations leading to this instability and find them to be of two different types. Close to the lower-amplitude threshold stable two-frequency quasiperiodic solutions exist surrounding the unstable stationary solution, and the dynamics remains trapped around the latter so that in particular the amplitude of the originally unexcited site remains small. By contrast, close to the higher-amplitude threshold all two-frequency quasiperiodic solutions are detached from the unstable stationary solution, and the resulting dynamics is of 'population-inversion' type involving also the originally unexcited site.

PACS numbers: 05.45.-a, 42.65.Sf, 63.20.Ry, 45.05.+x, 03.75.Fi

Submitted to: *J. Phys. A: Math. Gen.*

1. Introduction

As indicated by a number of recent results (e.g. [1, 2, 3, 4, 5, 6, 7, 8, 9]), oscillatory instabilities of time-periodic solutions in Hamiltonian anharmonic lattice models are quite ubiquitous, and are likely to play an important role in the general dynamics of any physical system which, in some approximation, can be described by such a model. Typically they are associated with an inhomogeneous amplitude distribution of the solution dividing the lattice into two sublattices of small- and large-amplitude sites, respectively, and oscillatory instabilities appear when internal oscillations of the sublattices resonate.

As long as the harmonic coupling is not too strong, time-periodic solutions for coupled anharmonic oscillators can be conveniently described using the multibreather formalism [10, 11], which utilizes the limit of zero coupling (anticontinuous limit) to identify each solution with a coding sequence. In the simplest case of time-reversible solutions with one single determination of the oscillation pattern for the individual uncoupled oscillators at a given time-period, the code is defined as +1 for each site which oscillates with this period and with a certain reference phase, -1 for each site oscillating with the opposite phase, and 0 for each site at rest. (As described e.g. in [11], this scheme can be readily generalized to include e.g. higher-harmonic oscillations by allowing codes $\pm 2, \pm 3, \dots$, or non-time-reversibility by allowing arbitrary phase torsions). This identification is unique for sufficiently weak coupling [10, 11], and can be readily obtained by numerical continuation using Newton-type schemes (e.g. [12]).

In particular, for Klein-Gordon (KG) chains of harmonically coupled soft anharmonic oscillators, most known examples of oscillatory instabilities have been associated with solutions whose multibreather coding sequences contain blocks of the kind $\dots, +1, 0^p, -1, 0, \dots$, with integer $p \geq 0$, or solutions bifurcating from such solutions (here 0^p means code 0 repeated p times). (For hard oscillators, a corresponding statement is true provided that the phase of every second oscillator is reversed by multiplying the code sequence with $(-1)^n$.) Thus, the essential ingredients providing the two-sublattice structure are large-amplitude sites of alternating phases with codes ± 1 and small-amplitude sites with codes 0. Generically, such solutions are linearly stable for weak enough coupling when the frequencies of internal oscillations for the two sublattices are well separated, but increasing the coupling yields a possibility for frequency overlap, and thereby resonances and instabilities. By contrast, blocks of the kind $\dots, +1, 0^p, +1, 0, \dots$ or $\dots, -1, 0^p, -1, 0, \dots$ typically yield nonoscillatory instabilities already for weak couplings. This difference can be related to the different natures of the extrema for a corresponding effective action, defined in [11] as a function of the individual phases at each site (see also [13, 14, 3], and [15] for further developments).

Particular examples of solutions where oscillatory instabilities have been explicitly demonstrated for not too small couplings include: (i) the two-site out-of phase breather with code $\dots 0, 0, 0, 1, -1, 0, 0, 0 \dots$ [1, 14] (also termed 'twisted localized mode' (TLM) [16, 5]); (ii) the 'discrete dark soliton' [3, 17, 7] ('dark breather' [9]) consisting of a

hole and a phase shift ('discommensuration') added to a stable background wave, with code ...+1, -1, +1, -1, 0, +1, -1, +1, -1, ...; (iii) nonlinear standing-wave (SW) phonons [4, 7, 8], corresponding to periodic or quasiperiodic repetitions of blocks of codes of type $\{1, 0^p, -1, 0^q\}$ with particular combinations of integers $p, q \geq 0$. In particular the latter instabilities are believed to play an important role in the processes of breather formation and evolution to energy equipartition [7, 8]. Also in higher dimensions oscillatory instabilities have been found for certain multibreather configurations, such as the two-dimensional discrete localized vortices [13, 18, 6].

Mathematically, the oscillatory instabilities appear through collisions of eigenvalues to the corresponding linearized eigenequations which have opposite Krein signatures, often called 'Krein collisions' (e.g. [19]) or 'Krein crunches'. Although well-known from many other branches of physics, the relevance of such collisions for the dynamics of anharmonic lattices was realized mainly after their reinterpretation in [11]. Generally the linear stability of time-periodic solutions is studied through the linearization of a Poincaré return map with the exact solution as a fixed point (Floquet map), and the symplectic nature of this map implies that all eigenvalues (Floquet multipliers) must lie on the unit circle for stability. A Krein collision then corresponds to four eigenvalues leaving the unit circle as a complex quadruplet.

However, it is wellknown that for KG lattices with weak inter-site coupling, the small-amplitude dynamics is well described by a discrete nonlinear Schrödinger (DNLS) equation which can be derived through a multi-scale expansion (e.g. [20, 7]). Within this approximation any time-periodic solution of the original KG model becomes a purely harmonic (stationary) solution of the DNLS model, and moreover by studying the dynamics in a frame rotating with this frequency, the DNLS solution becomes time-independent. Thus, by performing also the stability analysis of the DNLS solution in the rotating frame, the problem is reduced to the simpler problem of studying the stability of (relative) equilibria, as no explicit time-dependence appears in the linearized equations [21, 22]. Linear stability then demands all eigenvalues of the linearized flow to lie on the imaginary axis, and a Krein collision manifests itself as two pairs of complex conjugated eigenvalues on the imaginary axis with opposite Krein signature colliding and going out in the complex plane as a quadruplet (e.g. [23]). This collision is sometimes (e.g. [24, 25]) also referred to as a 1:-1 resonance (equal frequencies but opposite Krein signatures), and corresponds to a bifurcation of two families of time-periodic solutions which, due to its similarity to a Hopf bifurcation in dissipative systems, has been termed [26] a Hamiltonian Hopf (HH) bifurcation. (A description of the essential aspects of the HH bifurcation in more elementary terms was recently given in [27].) Note that since these families of solutions to the DNLS equation are time-periodic in a rotating frame, they generally correspond to quasiperiodic two-frequency solutions in the original frame. It is a special property of the DNLS equation (and other equations with particular symmetries [28]) that such quasiperiodic solutions may persist, and even be spatially localized, in the limit of infinite lattice size [10, 14, 5].

It is our purpose here to describe in some detail the nature of these bifurcations,

with the aim to obtain an increased understanding for the resulting dynamics in the regime of oscillatory instability. In this paper, we will focus on the simplest possible model where the above described mechanism for oscillatory instabilities can occur: the 3-site DNLS-model with periodic boundary conditions and the stationary solution with code $+1, -1, 0$. In a sequel to this paper, we will then analyze how these results extend to the above-mentioned examples for infinite lattices. The fact that this solution of the DNLS trimer model exhibits a complex instability is known already since the pioneering works of Eilbeck et.al. [21, 22]; however, it is somewhat surprising that, in spite of the wealth of existing literature on this model (e.g. [21, 22, 29, 30, 31, 32, 33, 34, 35] and references therein), to the very best of the knowledge of the present author the unstable dynamics of these stationary states and the properties of the surrounding quasiperiodic solutions were never before analyzed.

In addition to its importance in the approximate description of general anharmonic lattice dynamics, the DNLS model has many other particular applications (see e.g. [36, 37] for recent reviews), of which we here especially mention coupled optical waveguide arrays (e.g. [38, 39]) and coupled Bose-Einstein condensates (e.g. [40, 34, 35, 41]), both providing, due to the recent experimental developments in these fields, very exciting possibilities for practical utilization of the theoretical results.

The outline of this paper is as follow. In section 2 we define the DNLS model and describe the relevant stationary solutions and their linear stability properties (much of the material in this section is recapitulated from [21, 22]). In section 3 we use the technique described in [14] to calculate numerically families of exact quasiperiodic two-frequency solutions surrounding the stationary $\{1, -1, 0\}$ solution, and in particular we analyze the nature of the two HH bifurcations associated with Krein collisions for the stationary solution. Our most important result here is that we find these bifurcations to be of two different types, described rigorously in a general context in [24, 25] and which, using terminology from [27], we will call 'type I' and 'type II', respectively (in a related context, these two bifurcation classes were called 'hyperbolic regime' and 'elliptic regime', respectively [42]). In the type I bifurcation, which appears at the low-amplitude instability threshold for the stationary solution, stable quasiperiodic solutions exist close to (but away from) the stationary solution also in its unstable regime, while in the type II bifurcation, occurring at the high-amplitude instability limit, the bifurcating solutions annihilate each other so that no quasiperiodic solutions exist close to the unstable stationary solution. In section 4 we show that this has important consequences for the instability-induced dynamics of the $\{1, -1, 0\}$ solution which exhibits a new type of self-trapping transition: in the low-amplitude part of the unstable regime the dynamics remains trapped around the initial solution, while in the high-amplitude part the dynamics wanders away and also to a significant extent involves the initially unexcited site in a 'population-inversion' [43] type dynamics. Finally, section 5 concludes the paper.

We should also remark that, while this work was in progress, we became aware of the recent preprint [43] which, within the framework of describing the dynamics of

three coupled Bose-Einstein condensates, reports numerical simulations exhibiting self-trapping effects and 'population-inversion' dynamics similarly to what we observe here. Whenever appropriate we will discuss the relation between our results and those of [43].

2. The DNLS model, stationary solution and linear stability

We consider the following form of the DNLS equation

$$i\dot{\psi}_n + C(\psi_{n+1} + \psi_{n-1} - 2\psi_n) + |\psi_n|^2\psi_n = 0, \quad (1)$$

where we assume $C \geq 0$. The DNLS equation is the equation of motion for the Hamiltonian

$$H(\{i\psi_n\}, \{\psi_n^*\}) = \sum_{n=1}^N \left(C|\psi_{n+1} - \psi_n|^2 - \frac{1}{2}|\psi_n|^4 \right), \quad (2)$$

with canonical conjugated variables $\{i\psi_n\}, \{\psi_n^*\}$. In addition to the Hamiltonian, the DNLS equation has also a second conserved quantity, the norm $\mathcal{N} = \sum_{n=1}^N |\psi_n|^2$. We consider the trimer, $N = 3$, and impose the periodic boundary conditions $\psi_0 = \psi_3$, $\psi_4 = \psi_1$ thus considering a triangular configuration with identical coupling between all sites. Note that we consider the case of positive intersite coupling and negative (attractive) nonlinearity in (2), but in principle the general case can be recovered since changing the sign of C in (1) is equivalent to making the transformation $\psi_n \rightarrow (-1)^n e^{-i4Ct} \psi_n$, while the same transformation followed by a time reversal $t \rightarrow -t$ is equivalent to changing the sign of the nonlinearity. However, as we consider an odd number of sites, each such transformation must also be accompanied by a change of boundary conditions from periodic to antiperiodic. Thus, our model is not equivalent to that of [43] who considered a periodic three-site configuration with positive coupling and positive (repulsive) nonlinearity. In the latter case, the obtained solutions are equivalent to a subclass (antisymmetric under transformation $n \rightarrow n + 3$) of the solutions to (1) with $C > 0$ for a hexagonal geometry ($N = 6$) analyzed in [44]. We also note that when $C \neq 0$, it can be normalized to $C = 1$ through the transformation $\psi_n \rightarrow \sqrt{C}\psi_n$, $t \rightarrow t/C$.

A time-periodic, stationary solution to (1) with frequency Λ has the form

$$\psi_n^{(\Lambda)}(t) = \phi_n^{(\Lambda)} e^{i\Lambda t} \quad (3)$$

with time-independent amplitudes $\phi_n^{(\Lambda)}$. The index (Λ) indicates the frequency-dependence of the amplitudes. We will consider the particular family of solutions with the structure $\{\phi_n^{(\Lambda)}\} = \{A, -A, 0\}$, where the amplitude A is related to the frequency Λ as

$$A = \sqrt{\Lambda + 3C}; \quad \Lambda > -3C. \quad (4)$$

For these solutions, we can then write the norm as

$$\mathcal{N} = 2A^2 = 2(\Lambda + 3C) \quad (5)$$

and the Hamiltonian as

$$H = A^2(6C - A^2) = 9C^2 - \Lambda^2 = \frac{\mathcal{N}}{2} \left(6C - \frac{\mathcal{N}}{2} \right). \quad (6)$$

Small-amplitude perturbations ϵ_n to stationary solutions can be analyzed by writing $\psi_n(t) = \left(\phi_n^{(\Lambda)} + \epsilon_n(t) \right) e^{i\Lambda t}$ and linearizing:

$$i\dot{\epsilon}_n + C(\epsilon_{n+1} + \epsilon_{n-1} - 2\epsilon_n) + 2|\phi_n^{(\Lambda)}|^2\epsilon_n + (\phi_n^{(\Lambda)})^2\epsilon_n^* - \Lambda\epsilon_n = 0. \quad (7)$$

For real $\phi_n^{(\Lambda)}$ a linear eigenvalue problem can be obtained by writing $\epsilon_n = a_n e^{-i\omega_1 t} + b_n^* e^{i\omega_1^* t}$, yielding

$$\begin{aligned} (2C + \Lambda - 2(\phi_n^{(\Lambda)})^2)a_n - C(a_{n+1} + a_{n-1}) - (\phi_n^{(\Lambda)})^2 b_n &= \omega_1 a_n \\ (\phi_n^{(\Lambda)})^2 a_n + C(b_{n+1} + b_{n-1}) - (2C + \Lambda - 2(\phi_n^{(\Lambda)})^2)b_n &= \omega_1 b_n. \end{aligned} \quad (8)$$

Then, linear stability is equivalent to having all eigenfrequencies ω_1 real. For some purposes it is more convenient to work with the linear combinations $U_n = a_n + b_n$, $W_n = a_n - b_n$ so that (8) becomes

$$\begin{aligned} \mathcal{L}_0 W_n &\equiv (2C + \Lambda - (\phi_n^{(\Lambda)})^2)W_n - C(W_{n+1} + W_{n-1}) = \omega_1 U_n \\ \mathcal{L}_1 U_n &\equiv (2C + \Lambda - 3(\phi_n^{(\Lambda)})^2)U_n - C(U_{n+1} + U_{n-1}) = \omega_1 W_n. \end{aligned} \quad (9)$$

The usefulness of this formulation of the linear eigenvalue problem becomes clear by noting that, if ϵ_n is expanded in its real and imaginary parts $\epsilon_n = \epsilon_n^{(r)} + i\epsilon_n^{(i)}$, (7) can be written in the Hamiltonian form

$$\begin{pmatrix} \{\epsilon_n^{(r)}\} \\ \{\epsilon_n^{(i)}\} \end{pmatrix} = \begin{pmatrix} 0 & \mathcal{L}_0 \\ -\mathcal{L}_1 & 0 \end{pmatrix} \begin{pmatrix} \{\epsilon_n^{(r)}\} \\ \{\epsilon_n^{(i)}\} \end{pmatrix} \quad (10)$$

where \mathcal{L}_0 and \mathcal{L}_1 defined by (9) are symmetric. Then, if $i\omega_1$ is a purely imaginary eigenvalue of (10) with $\omega_1 > 0$, the corresponding eigenvector is $\begin{pmatrix} \{U_n\} \\ \{iW_n\} \end{pmatrix}$ where (U_n, W_n) is the (real) solution of (9) with eigenfrequency ω_1 . Thus, to each real eigenfrequency $\omega_1 > 0$ of (8) and (9) we can associate a Krein signature $\mathcal{K}(\omega_1)$ from the symplectic product of the corresponding eigenvector with eigenvalue $i\omega_1$ of (10) with itself, which, using the standard sign convention as in e.g. [45], reads

$$\mathcal{K}(\omega_1) = \text{sign} \sum_n [U_n W_n + W_n U_n] = \text{sign} \sum_n [|a_n|^2 - |b_n|^2]. \quad (11)$$

With this sign convention, the Krein signature is the same as the sign of the (Hamiltonian) energy carried by the linear eigenmode [45]. (It should be noted that in a remark in an earlier publication [46], we had used an opposite sign convention.)

Due to the invariance of the DNLS equation under global phase rotations, $\omega_1 = 0$ is always an eigenvalue of algebraic multiplicity 2 and geometrical multiplicity 1, and the corresponding solution is $U_n = 0, W_n = \phi_n^{(\Lambda)}$ ('phase mode'). For the particular solutions $\{\phi_n^{(\Lambda)}\} = \{A, -A, 0\}$ with A given by (4), the remaining eigenfrequencies are obtained [21] as

$$\left(\frac{\omega_1}{C} \right)^2 = \frac{1}{2} \left(\frac{\Lambda}{C} + 4 \right)^2 + 4 \pm \frac{1}{2} \sqrt{\left(\frac{\Lambda}{C} - 6 \right) \left(\left(\frac{\Lambda}{C} \right)^3 + 6 \left(\frac{\Lambda}{C} \right)^2 + 4 \frac{\Lambda}{C} - 24 \right)}. \quad (12)$$

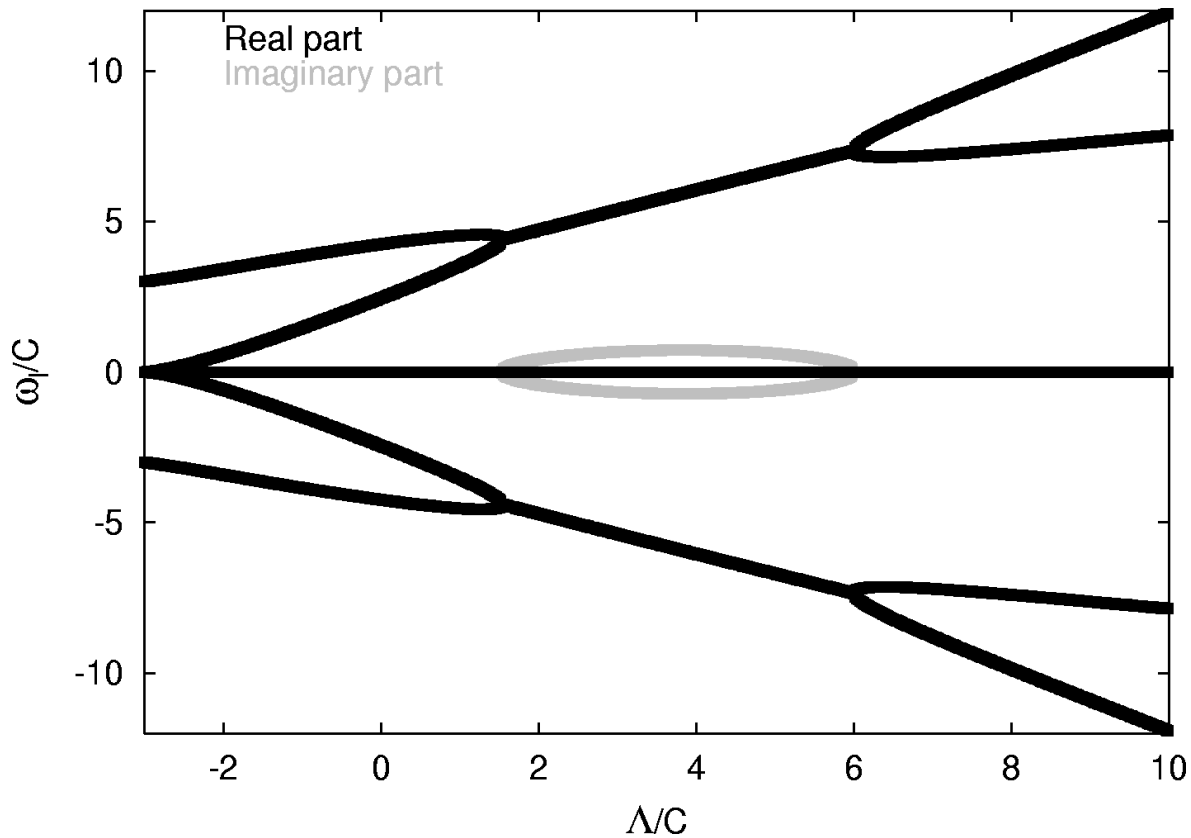


Figure 1. Scaled eigenfrequencies ω_1/C of the linear eigenvalue problems (8), (9) as a function of the scaled frequency Λ/C of the stationary solution described by (3)-(6). Dark (grey) lines represent real (imaginary) parts of ω_1/C .

The variation of the eigenfrequencies with the frequency Λ of the stationary solution is illustrated in figure 1. The eigenfrequencies are real close to the linear limit $\Lambda/C \rightarrow -3$ as well as close to the anticontinuous limit $\Lambda/C \rightarrow \infty$, but complex in the regime $x_* < \Lambda/C < 6$ where $x_* \approx 1.5385$ is the only real solution to $x^3 + 6x^2 + 4x - 24 = 0$ [21, 22]. Close to the linear limit we can expand (12) using $\lambda = A^2/C = \Lambda/C + 3 = \mathcal{N}/2C$ as a small parameter, and obtain the eigenfrequencies $|\omega_{1+}|/C \approx 3 + \lambda/3 + 4\lambda^2/27$ and $|\omega_{1-}|/C \approx 2\lambda^{3/2}/3$. For ω_{1+} the corresponding eigenmode can be expressed as

$$\left\{ \begin{pmatrix} a_n \\ b_n \end{pmatrix} \right\} = \left\{ \begin{pmatrix} -2\lambda/9 \\ 1 + 2\lambda/3 \end{pmatrix}, \begin{pmatrix} -2\lambda/9 \\ 1 + 2\lambda/3 \end{pmatrix}, \begin{pmatrix} \lambda/9 \\ 1 \end{pmatrix} \right\} + \mathcal{O}(\lambda^2) \quad (13)$$

and we have $\mathcal{K}(\omega_{1+}) = -1$, while for ω_{1-} the eigenmodes are most conveniently described as

$$\left\{ \begin{pmatrix} U_n \\ W_n \end{pmatrix} \right\} = \left\{ \begin{pmatrix} 1 \\ \sqrt{\lambda} \end{pmatrix}, \begin{pmatrix} 1 \\ \sqrt{\lambda} \end{pmatrix}, \begin{pmatrix} -2 - 2\lambda \\ -2\sqrt{\lambda} \end{pmatrix} \right\} + \mathcal{O}(\lambda^{3/2}) \quad (14)$$

with $\mathcal{K}(\omega_{1-}) = +1$. On the other hand, close to the anticontinuous limit we obtain from (12) when Λ/C is large the eigenfrequencies $|\omega_{1+}|/C \approx \Lambda/C + 2$ and $|\omega_{1-}|/C \approx$

$2\sqrt{\Lambda/C} + 5\sqrt{C/\Lambda}$. Then, we can write the corresponding eigenmode for ω_{1+} as

$$\left\{ \begin{pmatrix} a_n \\ b_n \end{pmatrix} \right\} = \left\{ \begin{pmatrix} 0 \\ C/\Lambda \end{pmatrix}, \begin{pmatrix} 0 \\ C/\Lambda \end{pmatrix}, \begin{pmatrix} 1 \\ 0 \end{pmatrix} \right\} + \mathcal{O}((C/\Lambda)^2) \quad (15)$$

with $\mathcal{K}(\omega_{1+}) = +1$, and the eigenmode corresponding to ω_{1-} as

$$\left\{ \begin{pmatrix} U_n \\ W_n \end{pmatrix} \right\} = \left\{ \begin{pmatrix} -\sqrt{C/\Lambda} \\ 1 \end{pmatrix}, \begin{pmatrix} -\sqrt{C/\Lambda} \\ 1 \end{pmatrix}, \begin{pmatrix} 0 \\ 2C/\Lambda \end{pmatrix} \right\} + \mathcal{O}((C/\Lambda)^{3/2}) \quad (16)$$

with $\mathcal{K}(\omega_{1-}) = -1$. Thus, the Krein signatures of the frequencies ω_{1+} and ω_{1-} are interchanged by the two Krein collisions at the boundaries of the complex regime, where the stationary solution is unstable (and the Krein signature undefined). Note also that the eigenmodes corresponding to nonzero frequencies are symmetric around the site $n = 3$, and thus their excitation breaks the spatial antisymmetry of the stationary solution around this site.

Let us finally in this section remark that if we consider the above stationary solution as periodically repeated in an infinite lattice, it becomes identical to a standing-wave phonon with wave vector $Q = 2\pi/3$ of 'type H' using the terminology of [4, 7, 8], and the eigenfrequencies (12) are the subset of all eigenfrequencies of the solution for the infinite system which correspond to spatially periodic eigenmodes of period 3. Close to the linear limit the mode (13) can then be interpreted as a phonon mode with wave vector $q = 0$, while the mode (14) represents a translational mode of wave vector $q = 2\pi/3$ corresponding to a sliding of the stationary solution towards the 'type E' $Q = 2\pi/3$ standing wave having a periodic repetition of the codes +1,-1,-1. Close to the anticontinuous limit the mode (15) represents a 'hole mode' localized at the zero-amplitude site of the stationary solution, while the mode (16) corresponds to an internal oscillation of the amplitudes of the sites with non-zero amplitude. In the intermediate, unstable, regime, these characters of the eigenmodes become mixed.

3. Two-frequency solutions: bifurcations and linear stability

When the eigenfrequencies ω_l of the linear equation (7) given by (12) are real and nonzero, they correspond to exact solutions to the fully nonlinear DNLS equation (1), which are time-periodic with period $T = 2\pi/\omega_l$ in the frame rotating with the stationary frequency Λ . In general, as described in some detail in [14], we can obtain such two-frequency solutions (which are generally quasiperiodic in the original frame) from the ansatz

$$\psi_n(t) = \phi_n(t)e^{i\omega_0 t}, \quad (17)$$

so that in the variables ϕ_n the DNLS equation (1) becomes

$$i\dot{\phi}_n + C(\phi_{n+1} + \phi_{n-1} - 2\phi_n) + |\phi_n|^2\phi_n - \omega_0\phi_n = 0. \quad (18)$$

Thus, the frequency ω_0 which corresponds to a pure rotation in the complex plane becomes a parameter in (18), and for a given ω_0 we search for time-periodic solutions

to (18) with frequency ω_b fulfilling $\phi_n(t + 2\pi/\omega_b) = \phi_n(t)$. In particular, any stationary solution to (1) of the form (3) is trivially a time-periodic solution to (18) of the form $\phi_n(t) = \phi_n^{(\Lambda)} e^{i\omega_b t}$ with frequency $\omega_b = \Lambda - \omega_0$. Then, when the condition $\omega_1(\Lambda) + \omega_0 = \Lambda$ is fulfilled for some real linear frequency ω_1 whose Λ -dependence is given by (12), families of genuine two-frequency solutions, which in the limit of small-amplitude oscillations around the stationary solution have frequencies $\omega_b = \omega_1$ in the rotating frame and coincide with the linear eigenmodes, bifurcate from the stationary solutions. Using standard numerical continuation techniques [14], these families of two-frequency solutions can be continued versus ω_b towards larger oscillation amplitudes away from the stationary solutions, and explicitly calculated to arbitrary precision in their whole domain of existence.

When performing the numerical continuation, one should pay particular attention to the conserved quantities. In fact, for an exact two-frequency solution there is, in addition to the norm and Hamiltonian which are always conserved, also a third constant of the motion which corresponds to the action ('area') integral I of the time-periodic solution to (18), i.e. in the frame rotating with frequency ω_0 . Using in this frame the canonical variables $\{i\phi_n\}, \{\phi_n^*\}$, corresponding to a transformation of the original Hamiltonian H into $H' = H + \omega_0 \mathcal{N}$, the action integral becomes

$$I = \frac{1}{2\pi} \int_0^{2\pi/\omega_b} \sum_{n=1}^N \phi_n^* i \dot{\phi}_n dt = H'/\omega_b - \frac{1}{4\pi} \int_0^{2\pi/\omega_b} \sum_{n=1}^N |\phi_n|^4 dt. \quad (19)$$

For genuine two-frequency solutions I is an independent conserved quantity, while for a stationary solution for which $i\dot{\phi}_n = -\omega_b \phi_n$ it is simply proportional to the norm, $I = -\mathcal{N}$ (the minus-sign arises only because in terms of action/angle variables, frequencies are defined with a sign opposite to that of (3) and (17) (see e.g. [14] and section 4). Thus, the two-frequency solutions to (1) belong to two-parameter families, where the parameters can be chosen either as frequencies ω_0, ω_b , or as action/norm I, \mathcal{N} (C is not an independent parameter since it only yields a rescaling, thus we will put $C = 1$ in all numerical calculations). We will choose as independent parameters the frequency ω_b in the rotating frame and the norm \mathcal{N} , and perform the continuation versus ω_b for fixed norm by, at each value of ω_b , vary the parameter ω_0 in (18) so to obtain a solution with the desired value of \mathcal{N} (this procedure may fail at particular points if the dependence $\mathcal{N}(\omega_0)$ for solutions at fixed ω_b is nonmonotonous or multivalued; examples of this can be found below).

The linear stability of two-frequency solutions is obtained from the linearization of (18) around an exact time-periodic solution $\phi_n(t) = \phi_n^{(r)}(t) + i\phi_n^{(i)}(t)$ where $\phi_n^{(r)}$ and $\phi_n^{(i)}$ are real. The linearized equation for the small perturbation $\epsilon_n(t)$ will then have the same form as (7) with Λ replaced by ω_0 , and the real and constant $\phi_n^{(\Lambda)}$ replaced by a generally complex and time-periodic $\phi_n(t)$. Decomposing as in (10) also the perturbation into its real and imaginary parts, $\epsilon_n(t) = \epsilon_n^{(r)}(t) + i\epsilon_n^{(i)}(t)$, the linearized equations can be written

in Hamiltonian form as [21, 22]

$$\begin{pmatrix} \{\dot{\epsilon}_n^{(r)}\} \\ \{\dot{\epsilon}_n^{(i)}\} \end{pmatrix} = \begin{pmatrix} 0 & \mathbf{1} \\ -\mathbf{1} & 0 \end{pmatrix} \times \begin{pmatrix} \left(\omega_0 - 3(\phi_n^{(r)})^2 - (\phi_n^{(i)})^2 \right) \mathbf{1} - C\Delta & -2\phi_n^{(r)} \phi_n^{(i)} \mathbf{1} \\ -2\phi_n^{(r)} \phi_n^{(i)} \mathbf{1} & \left(\omega_0 - (\phi_n^{(r)})^2 - 3(\phi_n^{(i)})^2 \right) \mathbf{1} - C\Delta \end{pmatrix} \begin{pmatrix} \{\epsilon_n^{(r)}\} \\ \{\epsilon_n^{(i)}\} \end{pmatrix} \quad (20)$$

where $\mathbf{1}$ denotes the N -dimensional unit matrix and Δ the discrete Laplacian, $\Delta\epsilon_n = \epsilon_{n+1} + \epsilon_{n-1} - 2\epsilon_n$ (note that the second matrix in (20) is symmetric). Integrating (20) numerically over the period $T_b = 2\pi/\omega_b$ of ϕ_n yields the symplectic $2N \times 2N$ -dimensional Floquet matrix \mathbf{F}_{T_b} defined by

$$\begin{pmatrix} \{\epsilon_n^{(r)}(T_b)\} \\ \{\epsilon_n^{(i)}(T_b)\} \end{pmatrix} = \mathbf{F}_{T_b} \begin{pmatrix} \{\epsilon_n^{(r)}(0)\} \\ \{\epsilon_n^{(i)}(0)\} \end{pmatrix}, \quad (21)$$

and the solution $\phi_n(t)$ is linearly stable if and only if all eigenvalues α of \mathbf{F}_{T_b} lie on the unit circle. In the particular case of a stationary solution, the eigenvalues α of \mathbf{F}_{T_b} are related to the linear eigenfrequencies ω_1 of (8), (9) as $\alpha = e^{i2\pi\omega_1/\omega_b}$ with $\omega_b = \Lambda - \omega_0$.

For a genuine two-frequency solution there are two arbitrary phases, one corresponding to global phase rotations which we have chosen to be zero at $t = 0$ in the ansatz (17), and another corresponding to the phase of the time-periodic solution in the rotating frame $\phi_n(t)$ which we fix by choosing its imaginary part $\phi_n^{(i)}(0) = 0$ implying that the solution must be time reversible, $\phi_n^*(-t) = \phi_n(t)$. To each of these phase degeneracies there is a corresponding solution to the linearized equations (20) with period T_b , and thus a pair of eigenvalues $\alpha = +1$ of \mathbf{F}_{T_b} [14]. The first solution, corresponding to an infinitesimal global phase rotation, is $\epsilon_n(t) = i\phi_n(t)$ (i.e. $(\{\epsilon_n^{(r)}\}, \{\epsilon_n^{(i)}\}) = (\{-\phi_n^{(i)}\}, \{\phi_n^{(r)}\})$), while the solution corresponding to an infinitesimal translation of the phase in the rotating frame is $\epsilon_n(t) = \dot{\phi}_n(t)$ (i.e. $(\{\epsilon_n^{(r)}\}, \{\epsilon_n^{(i)}\}) = (\{\dot{\phi}_n^{(r)}\}, \{\dot{\phi}_n^{(i)}\})$). (Note that for stationary solutions, these become linearly dependent and there is only one pair of eigenvalues at $+1$.) Thus, for the particular case $N = 3$ that we consider here there is for a genuine two-frequency solution at most one pair of Floquet eigenvalues α not identical to $+1$, and thus the only way such a solution can change its stability is through collisions of the members of this pair either at $+1$ or at -1 .

Furthermore, because of the invariance of the DNLS equation and its linearization under the transformation $\phi_n \rightarrow -\phi_n$ and the antisymmetry ($\phi_2^{(\Lambda)} = -\phi_1^{(\Lambda)}$; $\phi_3^{(\Lambda)} = 0$) of the particular stationary solutions under consideration here, the families of two-frequency solutions bifurcating from these will have the additional space-time symmetry $\phi_1(t + T_b/2) = \phi_2(t)$, $\phi_3(t + T_b/2) = \phi_3(t)$ in the rotating frame. This implies that the time-periodic solution ϕ_n with $\phi_1(0) \neq \phi_2(0)$ will contain only odd harmonics of its fundamental frequency ω_b . As a consequence, collisions of Floquet eigenvalues at -1

corresponding to period-doubling bifurcations will not yield instabilities, which can be seen by decomposing the Floquet matrix as $\mathbf{F}_{\mathbf{T}_b} = \mathbf{P}_{1\leftrightarrow 2}\mathbf{F}_{\mathbf{T}_b/2}\mathbf{P}_{1\leftrightarrow 2}\mathbf{F}_{\mathbf{T}_b/2}$, where $\mathbf{F}_{\mathbf{T}_b/2}$ is the matrix obtained by integrating (20) over half a period and $\mathbf{P}_{1\leftrightarrow 2}$ interchanges sites 1 and 2. Thus, only collisions of eigenvalues β to $\mathbf{P}_{1\leftrightarrow 2}\mathbf{F}_{\mathbf{T}_b/2}$ at $\beta = \pm 1$ can yield instabilities, and they must all correspond to eigenvalue collisions at $\alpha = +1$ for the total Floquet matrix $\mathbf{F}_{\mathbf{T}_b}$ since $\alpha = \beta^2$. In our numerical analysis below, we will report the stability properties in terms of eigenvalues β rather than α .

3.1. The low-amplitude 'Type I' bifurcation

3.1.1. Small \mathcal{N}/C . Let us first discuss some properties of the two families of two-frequency solutions bifurcating from the stationary solution for $\Lambda/C < x_*$, i.e. $\mathcal{N}/C < 9.077\dots$. They correspond to the linear modes which have the asymptotic oscillation patterns given by (13) and (14), respectively, for small \mathcal{N}/C . The continuation of these modes versus ω_b for fixed $\mathcal{N}/C = 5$ is illustrated in figure 2. Notable features are, that the continuation from the stationary solution for both solutions is monotonous in the direction of decreasing ω_b , and that both solutions are linearly stable for a rather large interval of frequencies $\omega_b \leq \omega_{1\pm}$, but become strongly unstable at small ω_b (figure 2 (c)). For the grey solution in the figure, corresponding to ω_{1+} , the instability is caused by a collision of eigenvalues β at -1 producing a rapid and monotonous growth of the modulus of the negative eigenvalue β for small ω_b . This behaviour is typical for $\mathcal{N}/C > 4.5$. On the other hand, for $\mathcal{N}/C < 4.5$ the unstable negative eigenvalue β of the grey solution will attain a minimum value and then return again towards the unit circle, and finally through a collision at $\beta = -1$ the solution bifurcates into the homogeneous stationary solution with $\phi_1 = \phi_2 = \phi_3 = -\sqrt{\mathcal{N}/3}$, which is linearly stable in this regime [21, 22]. (The continuation versus ω_b is typically non-monotonous close to this bifurcation point.) At $\mathcal{N}/C = 4.5$ the homogeneous stationary solution becomes unstable [21], and by analyzing the dynamics of the grey solution in the limit $\omega_b \rightarrow 0$ for $\mathcal{N}/C > 4.5$, we find that it asymptotically approaches a (strongly unstable) solution consisting of homoclinic connections of unstable and stable manifolds of the homogeneous stationary solution (as further discussed in section 3.1.3, see also figure 9 (b) below).

The scenario for the black solution in figure 2, corresponding to ω_{1-} , is more complicated: it first becomes unstable through an eigenvalue collision at $\beta = +1$, which is also associated with a change of nature of the solution as can be seen in figure 2 (a). This behaviour is related to a third-harmonic resonance with the other (grey) two-frequency solution, and the eigenvalue collision appears at a value of ω_b close to (but not exactly at) $\omega_{1+}/3$. The instability first grows when decreasing further ω_b , but attains a maximum and finally, through a second collision at $+1$, the black solution at frequency ω_b becomes identical to the grey solution at frequency $3\omega_b$, which at that point is stable but becomes unstable through the collision at $\beta = -1$ slightly after. This final third-harmonic resonance occurs when $(\omega_b + \omega_0)_{\text{black}}$ for the black solution

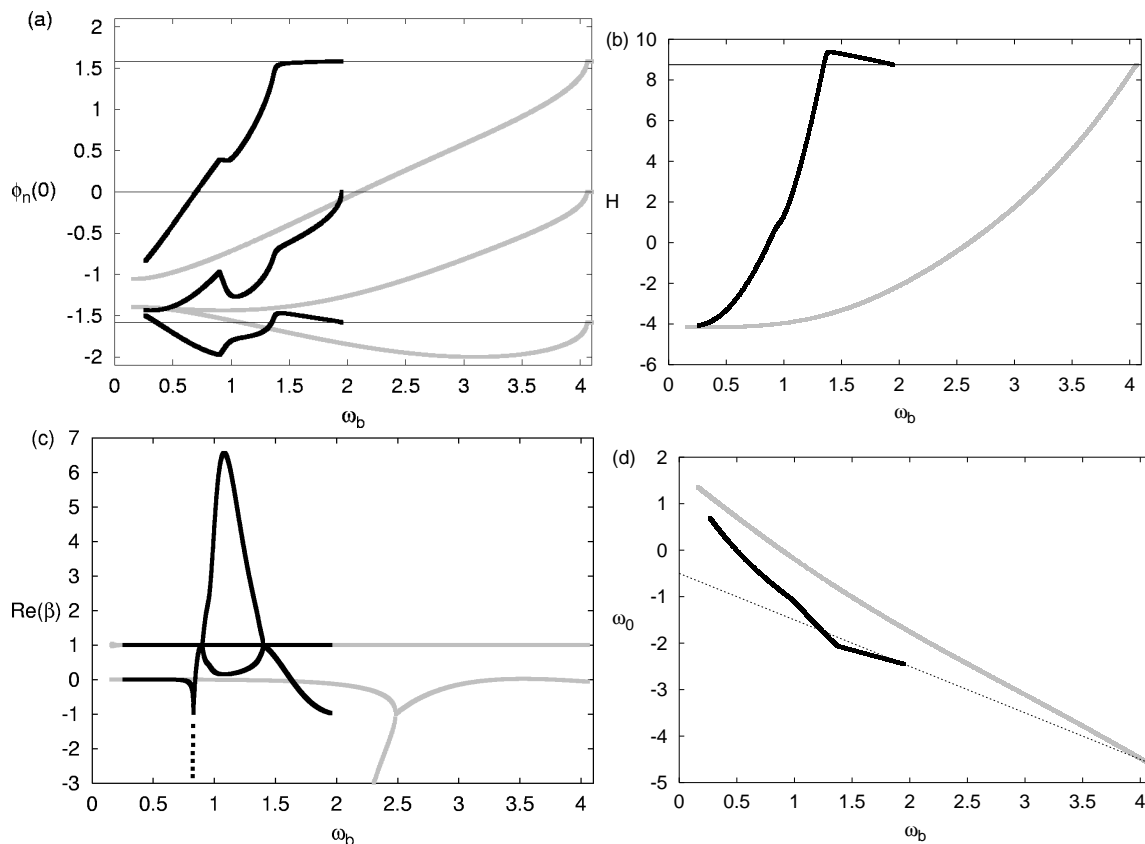


Figure 2. Continuation versus ω_b at fixed norm $\mathcal{N} = 5$ of the two two-frequency solutions bifurcating from the stationary solution (3)-(6) with $\Lambda = -0.5$ at frequencies $\omega_b = \omega_{1\pm}$ given by (12); black curves correspond to ω_{1-} and grey curves to ω_{1+} . (a) shows the initial amplitudes ϕ_n at time $t = 0$ for $n = 1$ (upper curves), $n = 2$ (lower curves) and $n = 3$ (middle curves); (b) shows the Hamiltonian H (2); (c) shows the real parts of the stability eigenvalues β of the matrix $\mathbf{P}_{1\leftrightarrow 2}\mathbf{F}_{\mathbf{T}_b/2}$, the square of which give the Floquet multipliers α ; (d) shows the frequency ω_0 of the rotating frame. The horizontal lines in (a) and (b) and the dashed line in (d) correspond to the stationary solution according to (4) and (6). The large negative eigenvalues not shown in (c) for small ω_b will continue to decrease rapidly (e.g. at $\omega_b = 0.2$ we find $\beta \approx -10^9$ for the grey solution). Note that the black solution for $\omega_b \lesssim 0.90$ is identical to the grey solution at frequency $3\omega_b$. ($C = 1$.)

becomes equal to $(\omega_b + \omega_0)_{\text{grey}}$ for the grey solution at the frequency $\omega_{b,\text{grey}} = 3\omega_{b,\text{black}}$. In general, for symmetry reasons such higher-harmonic resonances can occur only for odd harmonics as mentioned above. Since ω_{1-} decreases towards zero when \mathcal{N}/C decreases while ω_{1+} remains finite, for smaller \mathcal{N}/C the observed resonances will be of higher order. Thus, for example when \mathcal{N}/C approaches from above a critical value ~ 3.53 (where $\omega_{1+} = 3\omega_{1-}$) the value of ω_b where the black solution becomes unstable through the first collision at $\beta = +1$ associated with the third-harmonic resonance approaches the linear frequency $\omega_b = \omega_{1-}$, and for \mathcal{N}/C below this critical value the third-harmonic resonance disappears, and instead the solution will be stable until a fifth-harmonic resonance appears for smaller ω_b with an analogous scenario. It is interesting to note,

that if the continuation towards smaller ω_b is performed 'carelessly', i.e. with larger steps, one might 'jump' the regime yielding a p th harmonic resonance (p odd) and catch instead a solution in apparent (but non-smooth!) continuation of the original solution, as if the resonance had not existed. This solution can then be continued towards smaller ω_b until a $(p + 2)$ th harmonic resonance is encountered, etc. Thus, a cascade of higher-order resonances will result, and the scenario is analogous to that previously described for higher-order resonances in Klein-Gordon chains in [7] (see in particular figures 12 and 16 in this paper) and [48]. Furthermore, one also finds an even more complicated resonance scenario for the third-harmonic resonance as \mathcal{N}/C is increased. The behaviour shown in figure 2 is typical in the range $3.6 \lesssim \mathcal{N}/C \lesssim 5.5$, while for $\mathcal{N}/C \approx 5.6$ two additional eigenvalue collisions at $\beta = +1$ appear in the continuation towards smaller ω_b , slightly before the collision at $\beta = +1$ yielding the final transformation of the solution into the grey $3\omega_b$ -solution. Thus, a new pair of small regimes of stability/instability is produced. A further increase of \mathcal{N}/C yields even one more pair of small regimes of stability/instability through a collision at $\beta = -1$, and for $\mathcal{N}/C \gtrsim 6.8$ the continuation versus ω_b becomes nonmonotonous resulting in a 'Z-type' zig-zag-like continuation, where three different solutions of the family have the same frequency ω_b , in some regime before the final bifurcation with the $3\omega_b$ -solution (similar behaviour was also observed for the resonances in [7, 48]).

It is also interesting to note (figure 2 (b)), that the Hamiltonian of the black solution changes slope so that $dH/d\omega_b = 0$ at the first eigenvalue collision at $\beta = +1$ (but not at the second where the solution transforms to the grey third-harmonic solution). Moreover, the above-mentioned development of two additional eigenvalue collisions at $\beta = +1$ for $\mathcal{N}/C \approx 5.6$ also produces a nonmonotonous dependence $H(\omega_b)$ with a new pair of local min/max at the collision points. Generally (see also several similar examples below), it appears that $dH/d\omega_b = 0$ for two-frequency solutions at fixed norm could be a sufficient (but not necessary) condition for a change in stability through an eigenvalue collision at $+1$, analogous to the wellknown criteria $d\mathcal{N}/d\Lambda = 0$ for stationary solutions [47] and the more general $d\mathcal{I}/d\omega = 0$ for periodic solutions of Hamiltonian systems with frequency ω and action \mathcal{I} [25]. To formulate and prove such a condition rigorously would be an interesting mathematical issue, which however is beyond the scope of the present work.

3.1.2. Around the bifurcation point. We focus here on the regime of ω_b close to $\omega_{1\pm}$. A comparison of the solutions on both sides of the bifurcation point $\mathcal{N}/C \approx 9.077$ is shown in figure 3. Comparing the figures 3(a), (c), (e) for $\mathcal{N}/C = 9.07$ with figure 2, the most remarkable difference is that the continuation of the solution corresponding to the grey curves no longer is monotonous versus ω_b . Instead, the continuation from the stationary solution first goes in the direction of *increasing* ω_b from its linear value ω_{1+} up to a maximum value $\omega_b^{(\max)} \approx 4.5C$, from where the continuation turns and continues towards smaller ω_b similarly as above. Thus, this family of solutions is multivalued for $\omega_{1+} < \omega_b < \omega_b^{(\max)}$. This change of nature of the solution family occurs at $\mathcal{N}/C \approx 8.95$.

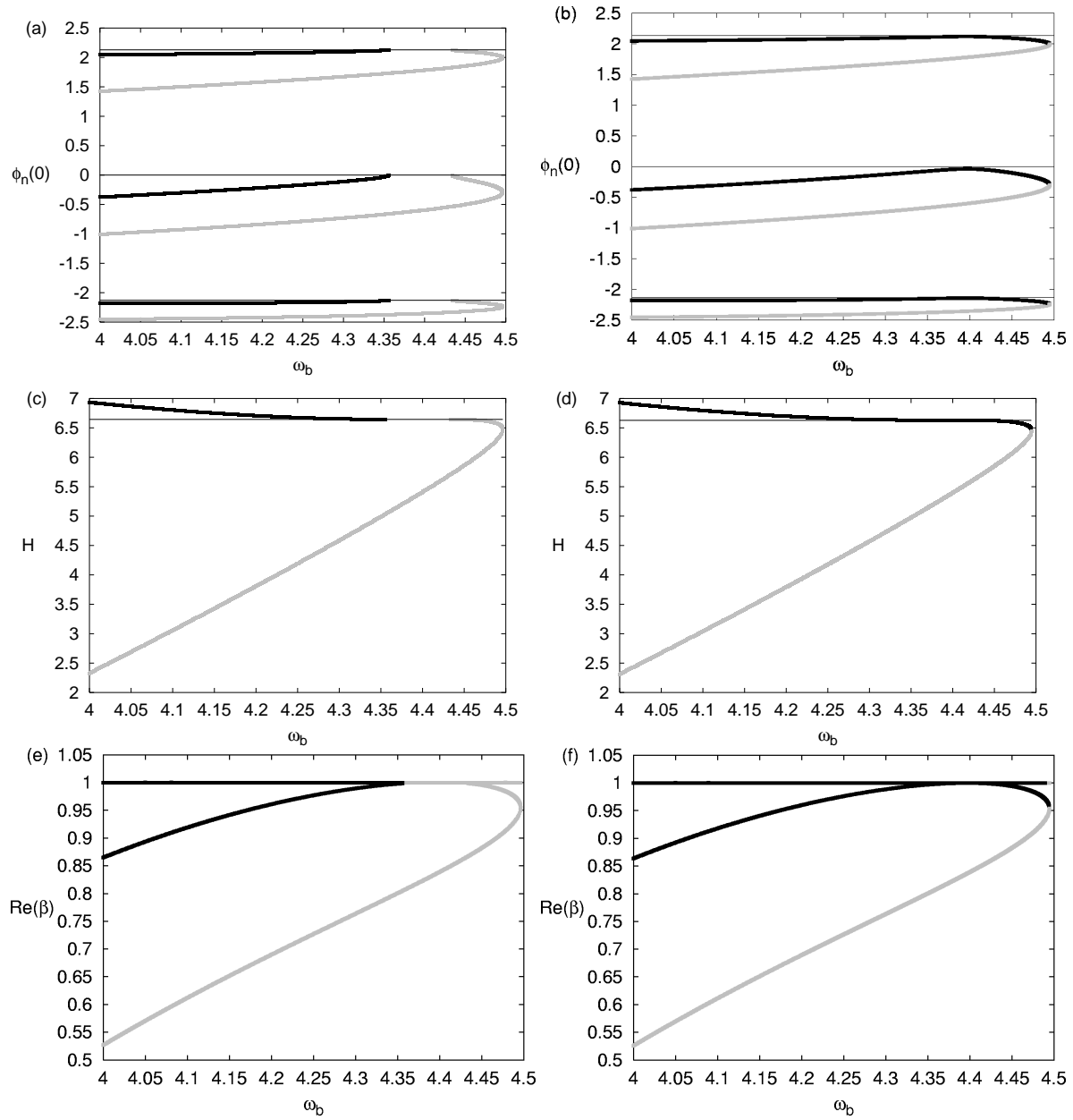


Figure 3. Same as figure 2 (a)-(c) but for $\mathcal{N} = 9.07$ (left figures) and $\mathcal{N} = 9.08$ (right figures). In (a), (c), (e) the meaning of the black and grey curves is the same as in figure 2, while in (b), (d), (f) they illustrate the two different but connected branches of coexisting two-frequency solutions continued from the solutions in the left figures.

In fact, as mentioned above, this multivaluedness of solutions causes numerical problems for the method of continuing for fixed norm by varying ω_0 at one point, where $d\mathcal{N}/d\omega_0$ for fixed ω_b becomes infinite (this point is generally different from, but close to, $\omega_b^{(\max)}$).

At the point of bifurcation $\mathcal{N}/C \approx 9.077$ the gap separating the two different families of solutions (black and grey in figure 3 (a), (c), (e)) closes (since $\omega_{1-} = \omega_{1+}$ at this point), and for larger \mathcal{N}/C as in figure 3 (b), (d), (f) they constitute two connected branches of a single family of two-frequency solutions which is now separated from the

stationary solution. It is of particular importance to note, that even though the two-frequency solutions are detached from the stationary solution on the superthreshold side of the bifurcation (where the latter is unstable and $\omega_{1\pm}$ are complex), it is clear from the scenario described by figure 3 that the distance between the two-frequency family and the stationary solution (which can be expressed in some suitable norm) decreases continuously to zero when approaching the bifurcation point from above. This is the characteristic property of a type I HH bifurcation as defined in [27], and close to the bifurcation point the scenario in figure 3 is equivalent to that of figure 2 in [27] (see also figure 2(b) in [24], [25]). The importance of this property for the dynamics of the unstable stationary solution will be illustrated in section 4.

3.1.3. Larger \mathcal{N}/C . When increasing \mathcal{N}/C on the superthreshold side of the type I bifurcation, the continued solutions will persist as two connected branches of a single family detached from the stationary solution from which they originally bifurcated, and continuously increase their distance to the latter. The typical behaviour of these solutions for larger \mathcal{N}/C is illustrated in figure 4 for $\mathcal{N}/C = 15$. Compared to the earlier discussed examples for smaller \mathcal{N}/C , we note two main differences. First, there is a small bubble of instability through a collision at $\beta = -1$ for the black solution in figure 4 (c) for $\omega_b \approx 2.9 - 3.0$. In fact, although not mentioned above such an instability occurs for the black solution in many regimes also for smaller \mathcal{N}/C (e.g. for $\mathcal{N}/C \gtrsim 5$), but it is then very weak and practically invisible numerically, while it grows considerably stronger for larger \mathcal{N}/C . Second, for $\mathcal{N}/C \gtrsim 9.45$ the black solution no longer transforms into the third-harmonic of the grey solution for small ω_b . Instead, as $\omega_b \rightarrow 0$ the black solution asymptotically approaches a (strongly unstable) solution with the same values of $\phi_n(0)$, H and ω_0 as the asymptotic grey solution (figure 4 (a), (b), (d)), but with $\beta \rightarrow +\infty$ while for the grey solution $\beta \rightarrow -\infty$ as before (figure 4 (c)). Thus, these asymptotic solutions are not identical, although they are both consisting of homoclinic connections of the unstable homogeneous stationary solution with $\phi_1 = \phi_2 = \phi_3$. This is possible since the latter has a doubly degenerate unstable eigenvalue [21], and thus the corresponding stable and unstable manifolds can be connected in different ways. Analysis of the dynamics yields that the grey solution in half a period contains two stable and two unstable manifolds from the homogeneous solution, and they are all associated with two-site localization with a third site of small $|\phi_n|^2$ as for $t = 0$ in figure 4 (a) (the small-amplitude site is $n = 1$, $n = 3$, $n = 2$ at times $t = 0$, $t = T_b/4$, $t = T_b/2$, respectively; cf. figure 9 (b) below). The black solution on the other hand contains three stable and three unstable manifolds in one half-period, and of these two pairs are associated with one-site localization with two sites of smaller $|\phi_n|^2$, and only one pair with two-site localization (the single large-amplitude site is $n = 1$ [$n = 2$] at $t = T_b/6$ [$t = T_b/3$], and the single small-amplitude site is $n = 1$ [$n = 2$] at $t = 0$ [$t = T_b/2$]; cf. figure 9 (a)).

We also note, by comparing figures 3 (d) and 4 (b), that while close to the bifurcation point the horizontal line representing the Hamiltonian for the unstable

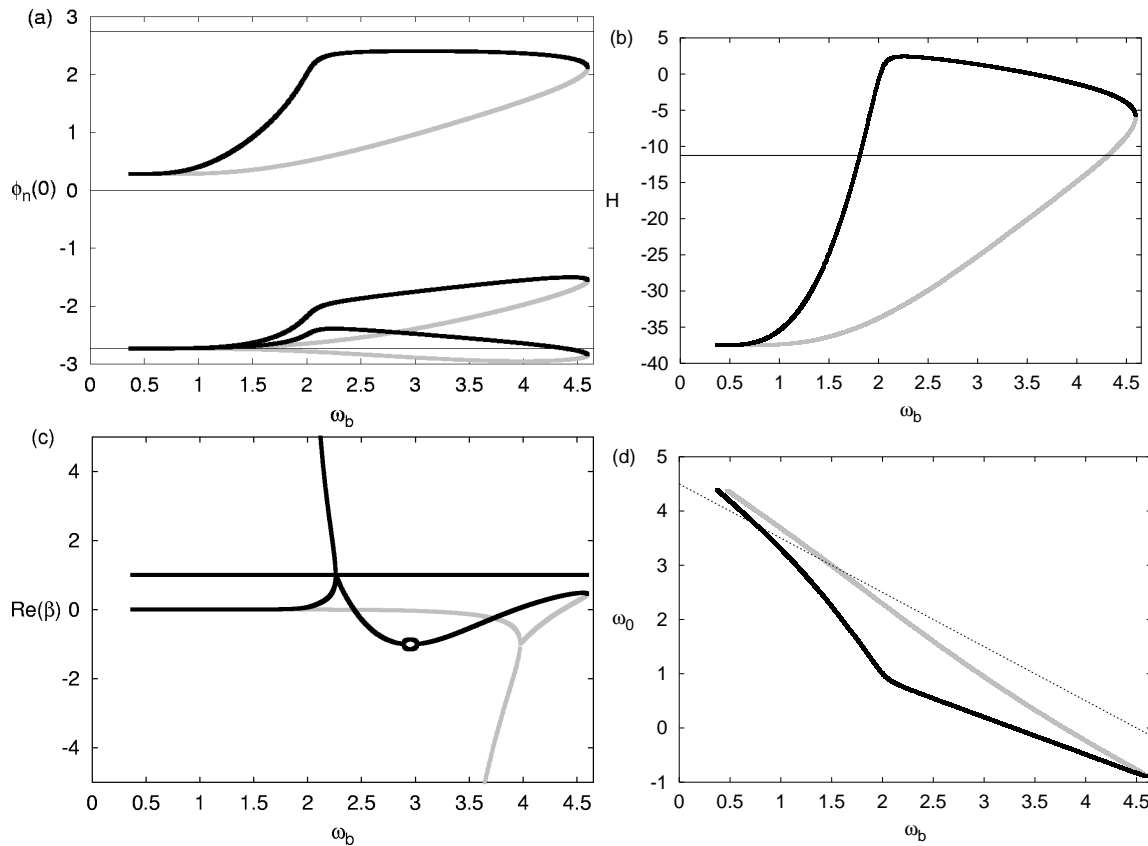


Figure 4. Continuation versus ω_b at fixed norm $\mathcal{N} = 15$ of the two-frequency solutions continued from the solutions in figures 2-3. The meaning of the black and grey parts is the same as in figure 3 (b), (d), (f); other quantities have the same meaning as in figure 2. The eigenvalues not shown in (c) for small ω_b will continue to decrease respectively increase monotonously for the grey and black solution; at $\omega_b = 0.5$ we find $\beta \approx -10^{12}$ for the grey solution and $\beta \approx 10^{11}$ for the black.

stationary solution (6) cuts the two-frequency solution family on the black branch (figure 3 (d)), the corresponding intersection point appears for larger \mathcal{N}/C on the grey branch (figure 4 (b)). This change of branch occurs at $\mathcal{N}/C \approx 10.6$, which, as will be discussed in section 4 below, is the value where the self-trapping transition of the unstable stationary solution is observed.

3.2. The high-amplitude 'Type II' bifurcation

Let us now turn our attention to the two-frequency solutions associated with the high-amplitude Krein collision for the stationary solution at $\Lambda/C = 6$, i.e. $\mathcal{N}/C = 18$. We start by describing some properties of these solutions on the stable side of the corresponding HH bifurcation, i.e. for $\mathcal{N}/C > 18$. It is important to note, as we will see, that these solutions are *not* identical to the solutions involved in the low-amplitude bifurcation described in the previous subsection.

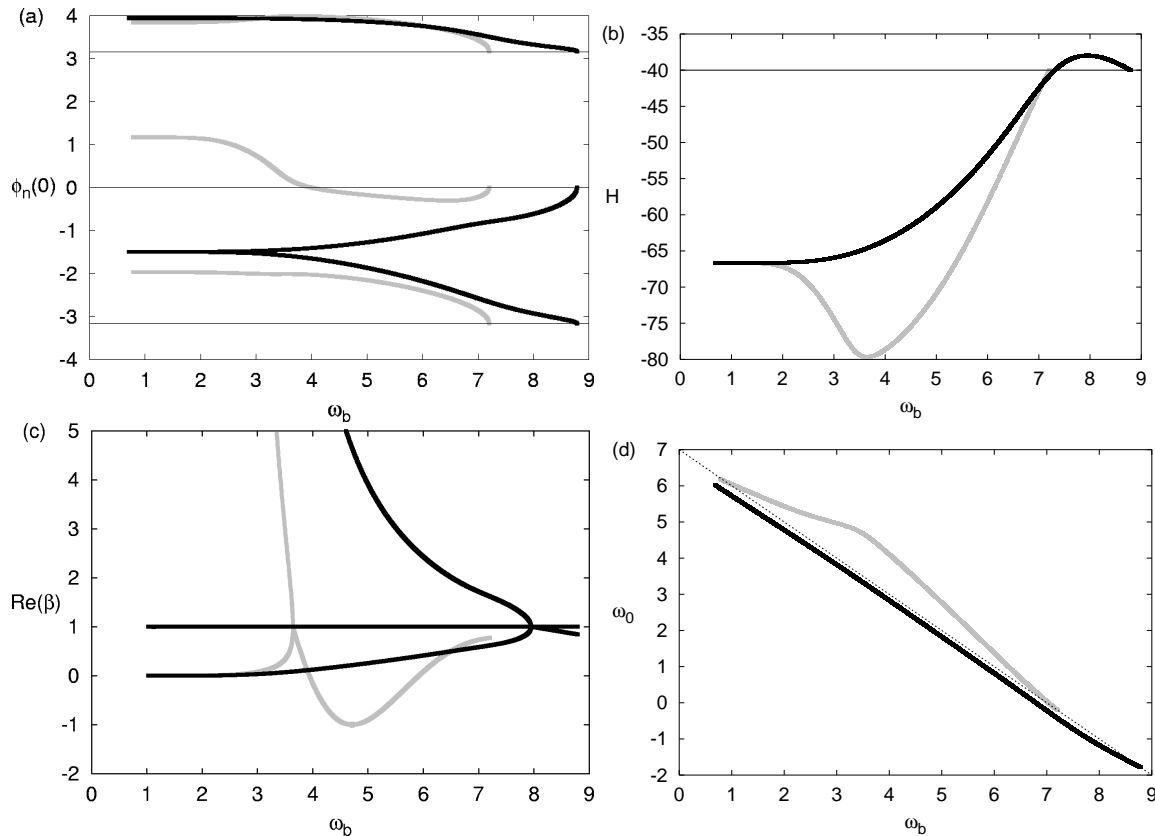


Figure 5. Same as figure 2 but for the families of two-frequency solutions bifurcating from the stationary solution with $\Lambda = 7$ at $\mathcal{N} = 20$; grey curves corresponding to solutions bifurcating at $\omega_b = \omega_{1-}$ and black curves to $\omega_b = \omega_{1+}$. The eigenvalues not shown in (c) for small ω_b will continue to increase monotonously for both solutions ($\beta \sim 10^8$ at $\omega_b = 0.8$).

3.2.1. Large \mathcal{N}/C . The continuation of the two families of two-frequency solutions corresponding to the linear modes which in the limit of large \mathcal{N}/C have asymptotic oscillation patterns given by (15) and (16), respectively, is shown in figure 5 for $\mathcal{N}/C = 20$. For both solutions the continuation from the linear modes is monotonous in the direction of decreasing ω_b , and similarly to the solutions discussed in section 3.1 they are both linearly stable in some regime of frequencies $\omega_b < \omega_{1\pm}$ but become strongly unstable for smaller ω_b ($\beta \rightarrow +\infty$ for both solutions as $\omega_b \rightarrow 0$; figure 5 (c)). The stability regime for the black solution in figure 5 is rather small, and in fact it is seen to be unstable in the whole frequency range where also the grey solution exists. We note also from figure 5 (b) that $dH/d\omega_b = 0$ at the instability thresholds occurring through collisions at $\beta = +1$ also here (there is also a tiny instability for the grey solution caused by collisions at $\beta = -1$ for $\omega_b \approx 4.70 - 4.73$ which does not reflect itself in the behaviour of $H(\omega_b)$). As $\omega_b \rightarrow 0$ also these two families of solutions will approach solutions consisting of homoclinic connections of stable and unstable manifolds of the homogeneous stationary solution $\phi_1 = \phi_2 = \phi_3$, which however are distinct both from each other and from those approached by the solutions described in section 3.1. Both

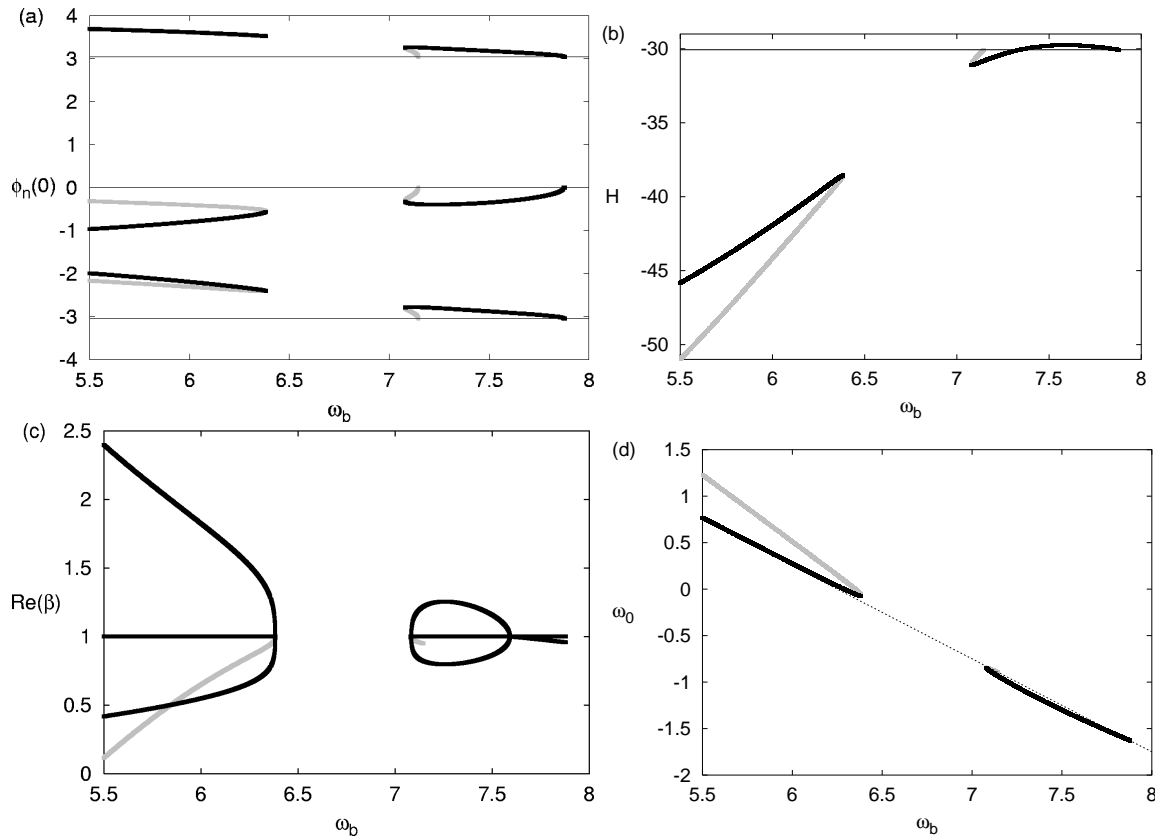


Figure 6. Same as figure 5 but for $\mathcal{N} = 18.5$. The black and grey curves are continuations of the corresponding solutions in figure 5. The behaviour for $\omega_b < 5.5$ not shown here is qualitatively the same as that of figure 5.

the asymptotic black and grey solutions in figure 5 contain one stable and one unstable manifold in each half-period, but while for the black solution the dynamics is of one-site-localization type with two sites of small equal $|\phi_n|^2$ (cf. figure 9 (c) below), the dynamics of the grey solution have all three sites of unequal amplitude as seen in figure 5 (a) (the large-amplitude site is $n = 1$ [$n = 2$] at $t = 0$ [$t = T_b/2$] for both solutions, and $n = 3$ is always a small-amplitude site; cf. figure 9 (d)).

3.2.2. Around the bifurcation point. When approaching from above the bifurcation point $\mathcal{N}/C = 18$ the frequencies ω_{1+} and ω_{1-} will approach each other, and moreover the corresponding families of two-frequency solutions (black and grey in figure 5) will approach each other as can be anticipated from figure 5. At $\mathcal{N}/C \approx 18.7$ the two solutions coincide at $\omega_b \approx 6.8$ ($< \omega_{1-} \approx 7.1$). At this point these two solutions bifurcate with each other, and compared to the scenario in figure 5 (c) an additional simultaneous collision at $\beta = +1$ appears for the black and grey solutions, in the regime where for larger \mathcal{N}/C the black solution was unstable and the grey stable. For smaller \mathcal{N}/C the solutions split into a low-frequency part and a high-frequency part separated by a forbidden gap in frequency ω_b as illustrated by figure 6 for $\mathcal{N}/C = 18.5$. Thus, only the high-frequency part is now connected to the stationary solution.

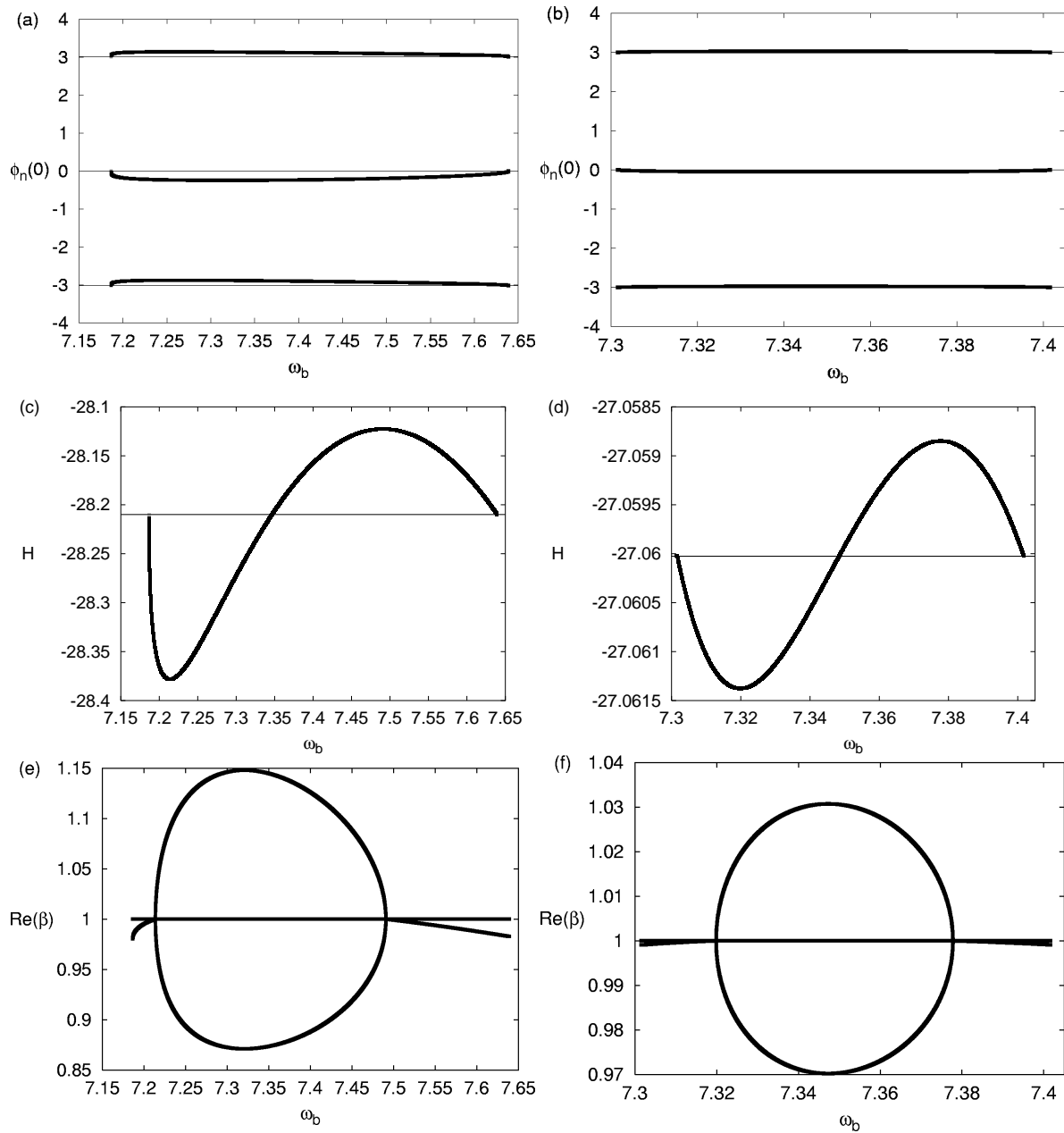


Figure 7. Continuation of the high-frequency branches of figure 6 (a)-(c) for $\mathcal{N} = 18.2$ (left figures) and $\mathcal{N} = 18.01$ (right figures). At $\mathcal{N} = 18.2$ there is still a tiny remainder of the grey part of previous figures which continues approximately 10^{-6} in the direction of negative ω_b from the linear value $\omega_b = \omega_{1-} \approx 7.186\,6898$.

For a further decrease of \mathcal{N}/C the loop constituting the high-frequency part will shrink as ω_{1+} and ω_{1-} approach each other, and furthermore at $\mathcal{N}/C \approx 18.2$ (figure 7 (a), (c), (e)) the continuation of the linear eigenmode of the stationary solution at $\omega_b = \omega_{1-}$ into the grey two-frequency solution changes direction to occur towards larger ω_b . Thus, in the regime $18 < \mathcal{N}/C \lesssim 18.2$ the high-frequency branch is univalued, and consists of one single family of solutions which through a monotonous continuation versus ω_b connects the linear eigenmode at ω_{1-} with that at ω_{1+} (figure 7 (b), (d), (f)).

The solutions on this branch are linearly stable close to the linear frequencies $\omega_b = \omega_{1\pm}$ but unstable for intermediate frequencies (figure 7 (f)) (note also the 'inverse N-shape' of $H(\omega_b)$ in figure 7 (d) which is consistent with the negative Krein signature of ω_{1-} and the positive of ω_{1+}). At the bifurcation point $\mathcal{N}/C = 18$, $\omega_{1-} = \omega_{1+}$ and the loop of surrounding two-frequency solutions shrinks to zero and vanishes. Consequently, for $\mathcal{N}/C < 18$ where the stationary solution is unstable, no nearby two-frequency solutions exist, and the scenario is that of a type II HH bifurcation as defined in [27] (cf. figure 3 in [27] and figure 2(a) in [24], [25]). However, the low-frequency branches in figure 6 still exist also for $\mathcal{N}/C < 18$, but at a considerable distance from the stationary solution (e.g. at $\mathcal{N} = 18$ and $C = 1$ the Hamiltonian (6) for the stationary solution is $H = -27$, while its maximum value on the disconnected branch of two-frequency solutions is $H \approx -39.4$). We illustrate the consequences of this for the dynamics of the unstable stationary solution in section 4.

3.2.3. Smaller \mathcal{N}/C . Continuing the low-frequency branches of figure 6 towards smaller \mathcal{N}/C , their features remain qualitatively the same. As an example we show in figure 8 these solution families for $\mathcal{N}/C = 15$. Comparison with figure 4 shows that, as previously stated, these solutions really are distinct from those originating from the low-amplitude bifurcation. Moreover, they remain at a large distance from the unstable stationary solution $\{\sqrt{\mathcal{N}/2}, -\sqrt{\mathcal{N}/2}, 0\}$ also when \mathcal{N}/C decreases (see e.g. the large difference in H in figure 8 (b)), and their maximum value of ω_b (i.e. the point where the black and grey branches meet) continues to decrease (e.g. at $\mathcal{N} = 10$ and $C = 1$ the solutions meet at $\omega_b \approx 2.33$).

To illustrate the different nature of the two solution branches of figure 4 and the two branches of figure 8 for small ω_b , we plot in figure 9 the resulting dynamics for one half-period $T_b/2$ (remembering that $\phi_1(t + T_b/2) = \phi_2(t)$, $\phi_3(t + T_b/2) = \phi_3(t)$ yields the complete dynamics) at $\omega_b = 0.58$. As ω_b decreases the flat parts of the curves will flatten and stretch out in time, so that as $\omega_b \rightarrow 0$ the previously described asymptotic solutions are approached. (We should remark that, since these solutions are strongly unstable, their accurate numerical determination even at $\omega_b = 0.58$ and for only half a period still requires working in quadruple precision.)

4. Instability-generated dynamics

Let us now discuss the dynamics resulting from initial conditions taken as a slightly perturbed stationary solution $\{\phi_n^{(\Lambda)}\} = \{\sqrt{\mathcal{N}/2}, -\sqrt{\mathcal{N}/2}, 0\}$ in various parts of its regime of Krein instability. We show three examples of such dynamics in figure 10. Figure 10 (a) for $\mathcal{N}/C = 10$, i.e. relatively close to the low-amplitude instability threshold, illustrates that in this regime the dynamics remains trapped forever in a state characterized by bounded oscillations around the initial unstable stationary solution. In particular, the amplitude of the initially unexcited site ($n = 3$) will always remain small compared to those of the other two sites. As \mathcal{N}/C increases the amplitude of these

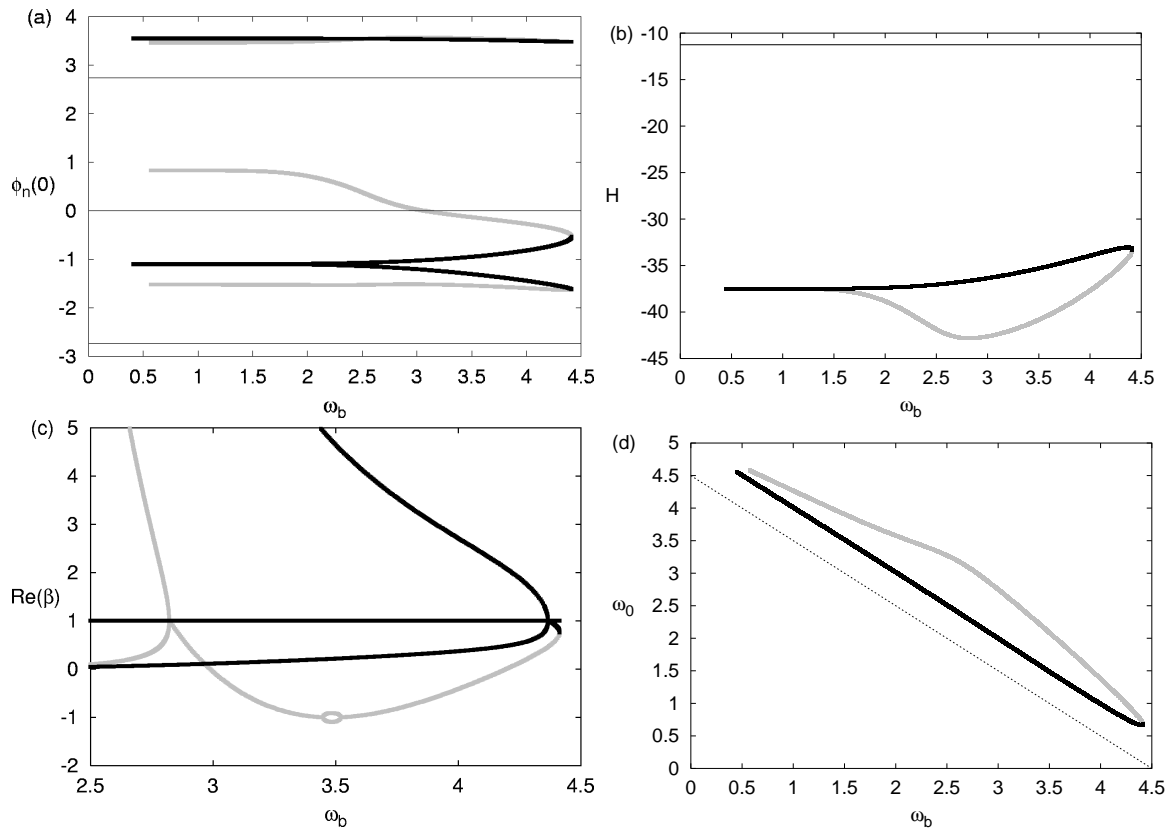


Figure 8. Continuation of the low-frequency branches of figure 6 for $\mathcal{N} = 15$. The eigenvalues not shown in (c) for small ω_b will continue to increase monotonously for both solutions ($\beta \sim 5 \cdot 10^6$ at $\omega_b = 0.8$). As in previous figures, the horizontal lines in (a), (b) and the dashed line in (d) show corresponding quantities for the (unstable) stationary solution $\{\sqrt{\mathcal{N}/2}, -\sqrt{\mathcal{N}/2}, 0\}$ ($C = 1$ as in all figures).

oscillations increases, and above a certain threshold value $\mathcal{N}/C \approx 10.6$ the self-trapping is destroyed and the dynamics of all three sites becomes qualitatively the same. The behaviour close to but above this value is illustrated in Figure 10 (b) for $\mathcal{N}/C = 11$. As can be seen, the dynamics is still trapped for some time, but finally after $t \sim 900$ the trapping is destroyed and the amplitude of the third site increases drastically. The length of the initial transient dynamics approaches infinity as \mathcal{N}/C approaches the self-trapping transition point ~ 10.6 , but decreases for increasing \mathcal{N}/C so that when approaching the high-amplitude instability threshold at $\mathcal{N}/C = 18$ no transient is observed (see figure 10 (c) for $\mathcal{N}/C = 17$). In all cases, the dynamics in the untrapped regime can be characterized as 'intermittent population inversion', which was observed also for certain initial conditions of the (nonequivalent) trimer model studied in [43]. This is most clearly seen in figure 10 (c). Here, one can during certain time intervals unambiguously identify two sites of large amplitude and a single small-amplitude site, which changes from initially being $n = 3$ to $n = 2$, and then, during a rather long time, to $n = 1$. After that follows a regime of more complicated oscillations, which then again is followed by a regime with a single small-amplitude site changing from $n = 3$ to $n = 1$ and then to

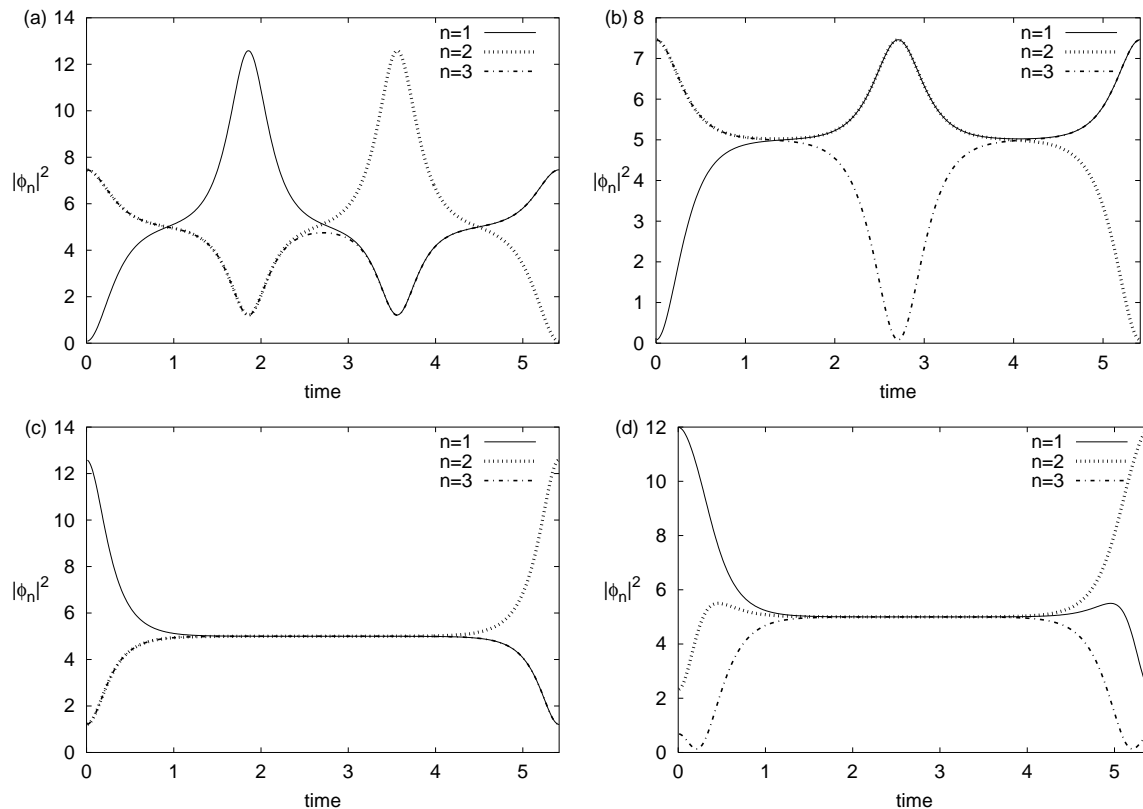


Figure 9. Dynamics for one half-period of the four different solutions in figures 4 and 8 at $\mathcal{N} = 15$, $\omega_b = 0.58$ and $C = 1$. (a) and (c) [(b) and (d)] correspond to the black [grey] solutions in figures 4 and 8, respectively.

$n = 2$, etc.

To understand more clearly the origin of this self-trapping transition, we analyze the dynamics close to the unstable stationary solution in terms of Poincaré sections. Such sections can of course be introduced in many different ways; here we apply similar ideas as in [30] making use of the transformation into action-angle variables $\{P_n, \theta_n\}$ defined by $\psi_n = \sqrt{P_n}e^{-i\theta_n}$ (a slightly different approach was used in [43]). It is then convenient to replace one of the action variables, which we here choose as P_1 , with the norm \mathcal{N} which is a conserved quantity. Then, the angle-variables conjugated to the set of generalized momenta $\{\mathcal{N}, P_2, P_3\}$ are [30] $\{\theta_1, \theta_2 - \theta_1, \theta_3 - \theta_1\}$, so that θ_1 describing an overall phase becomes an ignorable coordinate. Thus, the essential dynamics takes place in a four-dimensional space where the surface of constant energy H is three-dimensional, so that a proper Poincaré section through it becomes two-dimensional. Consequently, although chaotic trajectories may fill a large portion of the available phase space [22, 30], Arnold diffusion is prohibited [29, 49] since the presence of any regular KAM tori will disconnect the phase space. (Arnold diffusion does however appear for the four-site DNLS model [49, 50].)

As a particular choice of Poincaré section giving a clear illustration of the self-trapping transition, we choose to plot $P_3 = |\psi_3|^2$ versus $\theta_3 - \theta_1$ at each time instant

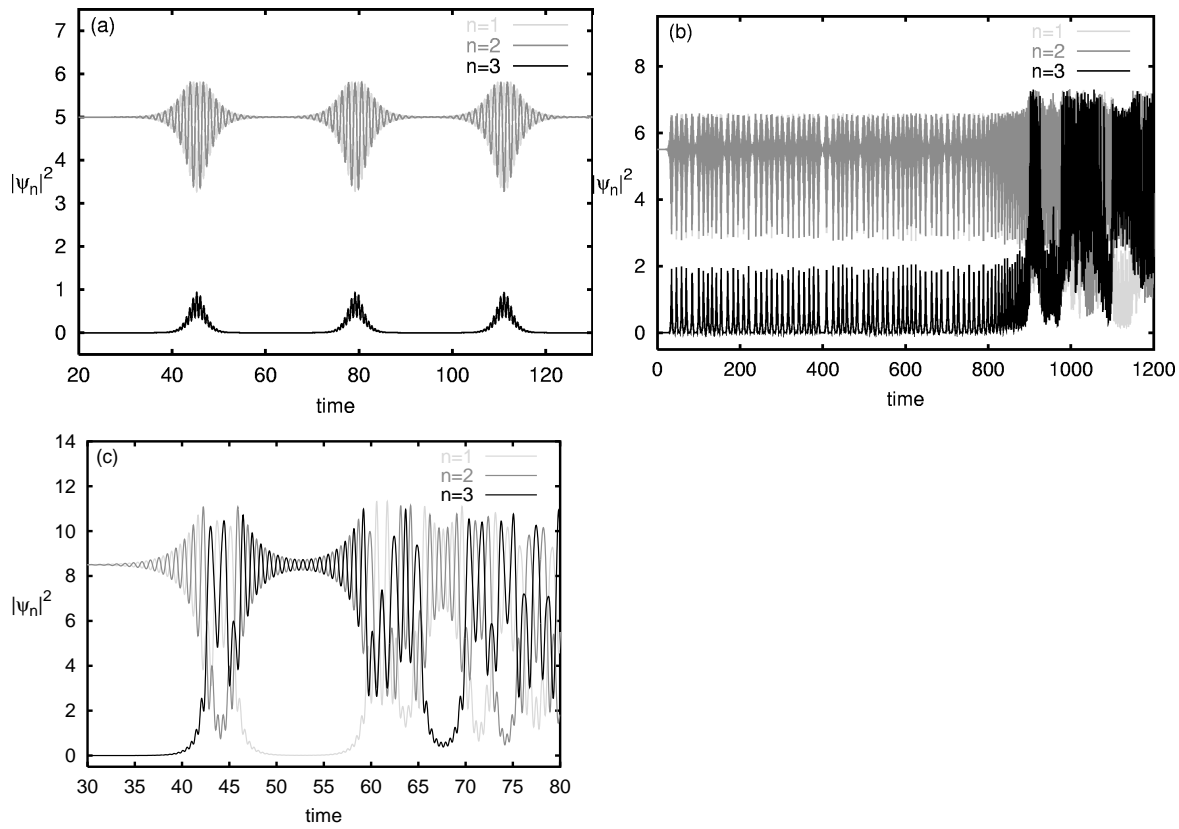


Figure 10. Typical instability-generated dynamics for randomly perturbed unstable stationary solutions (3)-(6) with $C = 1$ and (a) $\mathcal{N} = 10$, (b) $\mathcal{N} = 11$, and (c) $\mathcal{N} = 17$, respectively. The size of the initial perturbation is of the order of 10^{-8} .

when $\theta_2 - \theta_1 = \pi$ and $\frac{d}{dt}(\theta_2 - \theta_1) < 0$. Examples of such plots for parameter values on both sides of the self-trapping transition are shown in figure 11. Since the stationary solution has zero amplitude at the site $n = 3$ its phase θ_3 is undefined, and thus it is represented by a horizontal line $|\psi_3|^2 = 0$ in figure 11. The scenario in the self-trapped regime is illustrated by figure 11 (a), corresponding to the dynamics in figure 10 (a). Here the elliptic fixed point at $\theta_3 - \theta_1 = \pi$ represents the stable branch of the two-frequency solutions described in section 3.1. It can be seen from pictures similar to figure 3 (d), (f) that the relevant solution in this case is the one with the largest value of H (black line in these figures), which is stable at the point where its value of H is identical to that of the stationary solution. This elliptic fixed point appears at $|\psi_3|^2 = 0$ at the point of the type I HH bifurcation $\mathcal{N}/C \approx 9.077$, and moves vertically in the direction of increasing $|\psi_3|^2$ for increasing \mathcal{N}/C (cf. figure 3 (b)). For our purposes, it is most important to note that this fixed point is surrounded by two different kinds of regular periodic or quasiperiodic orbits, which in the latter case constitute KAM tori corresponding generically to quasiperiodic solutions with *three* incommensurate frequencies in the original DNLS dynamics. With a pendulum analogy, these orbits can be classified as 'rotating' and 'vibrating', respectively, where the rotating orbits extend for all values of $\theta_3 - \theta_1$ while the vibrating orbits only exist in a bounded region

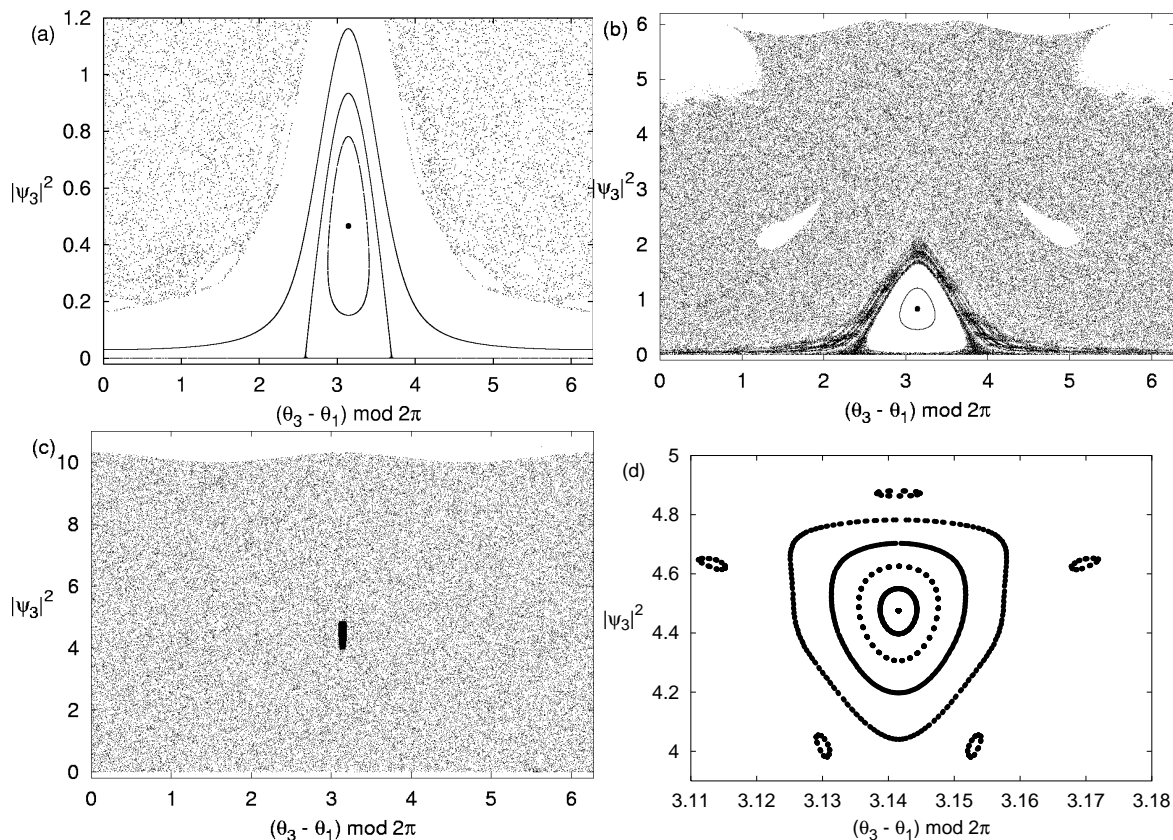


Figure 11. Poincaré sections $\theta_2 - \theta_1 = \pi$, $\frac{d}{dt}(\theta_2 - \theta_1) < 0$ for the dynamics close to unstable stationary solutions (3)-(6) with $C = 1$ and (a) $\mathcal{N} = 10$ ($H = 5$), (b) $\mathcal{N} = 10.7$ ($H = 3.4775$), and (c), (d) $\mathcal{N} = 17$ ($H = -21.25$), respectively. The stationary solution is in each figure represented by the horizontal line $|\psi_3|^2 = 0$. The elliptic fixed point illustrated by a filled circle represents the stable branch of the two-frequency solutions calculated in section 3.1 (continuations of solutions shown in figures 3-4). The window of regular trajectories in (d) is marked by a short vertical black line in (c).

close to $\theta_3 - \theta_1 = \pi$. Then, the unstable stationary solution becomes the separatrix between these different kinds of solutions. Although the separatrix is chaotic (which can be seen from a careful look at figure 11 (a)) the chaos is confined between KAM-tori, and in particular the existence of confining 'rotating' tori makes it impossible for $|\psi_3|^2$ to exceed some upper limit value ($|\psi_3|^2 \approx 1$ at $\theta_3 - \theta_1 = \pi$ in figure 11 (a)). Thus, self-trapping results.

Below the point of the type I HH bifurcation $\mathcal{N}/C \approx 9.077$, where the stationary solution is stable and the elliptic fixed point with nonzero $|\psi_3|^2$ is not yet born, all surrounding KAM tori are of the 'rotating' kind. As \mathcal{N}/C is increased and the elliptic fixed point moves upwards towards larger $|\psi_3|^2$, more and more of the 'rotating' KAM tori get destroyed, and finally at $\mathcal{N}/C \approx 10.6$ the last 'rotating' KAM torus breaks up, and the self-trapping is destroyed. The Poincaré plot for $\mathcal{N}/C = 10.7$, i.e. just above the transition point, is shown in figure 11 (b) (the corresponding dynamics is qualitatively similar to that of figure 10 (b) but with a longer transient time $t \sim 17000$). It can

be seen, that although the unstable stationary solution originating from the horizontal line $|\psi_3|^2 = 0$ finally will spread to a large part of the available phase space, the darker parts in the lower part of the figure signifies that the solution will be almost trapped in these regions for long times. This should be expected close to the transition point, as destroyed KAM tori should transform into cantori by a transition by breaking of analyticity [51]. Close to the transition the cantori should have almost full measure, and can thus trap the dynamics for very long times. (Note also the white parts in the upper part of the figure around $\theta_3 - \theta_1 = 0 \bmod 2\pi$; this is the region of dynamics trapped around the two-frequency solution with main amplitudes at sites $n = 2$ and $n = 3$, which is the counterpart to the elliptic fixed point at $\theta_3 - \theta_1 = \pi$ with dynamics trapped around $n = 1$ and $n = 2$.)

As mentioned in section 3.1.3, the self-trapping transition at $\mathcal{N}/C \approx 10.6$ is associated with a change of branch of the two-frequency solution family for which the Hamiltonian curve intersects that of the unstable stationary solution, so that for $\mathcal{N}/C \gtrsim 10.6$ the solution represented by the elliptic fixed point in figure 11 is the branch with the *lower* value of H (grey line in figure 4 (b)). For a further increase of \mathcal{N}/C the elliptic fixed point continues to move towards larger $|\psi_3|^2$ (cf. figure 4 (a)), and the surrounding island of stable KAM tori shrinks so that the unstable stationary solution invades almost all the available phase space. This is illustrated in figure 11 (c), (d) for $\mathcal{N}/C = 17$ (corresponding to the dynamics of figure 10 (c)). Here, there are no more any visible traces of the destroyed rotating KAM tori (if cantori exist they should be of very small measure), and consequently the dynamics in figure 10 (c) shows no transient trapping. This behaviour persists up to $\mathcal{N}/C = 18$, where the stationary solution becomes again stable through the type II HH bifurcation described in section 3.2. Before this, at $\mathcal{N}/C \approx 17.2$ the two-frequency solution yielding the elliptic fixed point in figure 11 (d) becomes unstable through a period-doubling type bifurcation (cf. the collision at $\beta = -1$ for the grey solution in figure 4 (c)), so that the elliptic fixed point becomes hyperbolic and splits into two new elliptic points with tiny KAM tori around them.

5. Conclusions

In conclusion, we have investigated in some detail the Hamiltonian Hopf bifurcations in the three-site DNLS model, resulting in a regime of oscillatory instability for the particular stationary solution with two sites of anti-phased oscillations and the third site of zero amplitude ('single depleted well' with the terminology of [43]). Using numerical continuation techniques to calculate the (generally quasiperiodic) two-frequency solutions involved in the bifurcations, we found the two bifurcations to be of two different types. At the low-amplitude instability threshold the bifurcation is of 'type I', implying the existence of stable two-frequency solutions close to the unstable stationary solution near the bifurcation point. These two-frequency solutions are themselves surrounded by KAM tori, representing generally quasiperiodic three-

frequency solutions of the full DNLS model. At the high-amplitude instability boundary, the HH bifurcation is of 'type II', and the stationary solution has no surrounding two-frequency solutions on the unstable side of the bifurcation. This reflects itself as a self-trapping transition in the instability-induced dynamics of the stationary solution, so that in the low-amplitude instability regime the dynamics remains trapped close to the initial state with small amplitude on the third site, while in the high-amplitude instability regime an 'intermittent population inversion' dynamics is observed with the small-amplitude oscillation moving chaotically between the sites. The self-trapping transition was found to correspond to the destruction of phase-space dividing KAM tori. As far as we are aware, this type of self-trapping transition has not been described earlier in the literature.

As discussed in the introduction, our original motivation for these studies was to obtain an increased understanding for the dynamics resulting from oscillatory instabilities of certain multibreather configurations in infinite lattices, which have been discovered recently in many contexts. Based on the results obtained here, we will address these issues in a forthcoming publication. However, the three-site DNLS model is of interest in itself, in particular in view of the recent experimental progress in the fields of coupled optical waveguides and Bose-Einstein condensates. It seems likely, that the existence of stable families of two-frequency solutions, corresponding to intensities periodically oscillating around their mean values, as well as the existence of a new type of self-trapping transition in the unstable dynamics of the stationary solution, should be experimentally verifiable within these contexts.

Acknowledgments

This work was initiated at the Seminar and Workshop on Nonlinear Lattice Structure and Dynamics, Dresden, Germany, September 03-30, 2001, and I thank the Max-Planck-Institut für Physik komplexer Systeme, and in particular Sergej Flach, for their hospitality. I also thank Chris Eilbeck for some helpful remarks, and for sending reprints of [44]. Parts of this work were inspired by earlier discussions with Serge Aubry. Financial support from the Swedish Research Council is also gratefully acknowledged.

References

- [1] Marín J L, Aubry S and Floría L M 1998 *Physica D* **113** 283–92
- [2] Marín J L and Aubry S 1998 *Physica D* **119** 163–74
- [3] Johansson M and Kivshar Yu S 1999 *Phys. Rev. Lett.* **82** 85–8
- [4] Morgante A M, Johansson M, Kopidakis G and Aubry S 2000 *Phys. Rev. Lett.* **85** 550–3
- [5] Kevrekidis P G, Bishop A R and Rasmussen K Ø 2001 *Phys. Rev. E* **63** 036603-1–6
- [6] Malomed B and Kevrekidis P G 2001 *Phys. Rev. E* **64** 026601-1–6
- [7] Morgante A M, Johansson M, Kopidakis G and Aubry S 2002 *Physica D* **162** 53–94
- [8] Johansson M, Morgante A M, Aubry S and Kopidakis G 2002 *Eur. Phys. J. B* **29** 279–83
- [9] Alvarez A, Archilla J F R, Cuevas J and Romero F R 2002 *New J. Phys.* **4** 72.1–19
- [10] MacKay R S and Aubry S 1994 *Nonlinearity* **7** 1623–43

- [11] Aubry S 1997 *Physica D* **103** 201–50
- [12] Marín J L and Aubry S 1996 *Nonlinearity* **9** 1501–28
- [13] Cretegny T and Aubry S 1997 *Phys. Rev. B* **55** R11929–32
- [14] Johansson M and Aubry S 1997 *Nonlinearity* **10** 1151–78
- [15] Ahn T, MacKay R S and Sepulchre J-A 2001 *Nonlinear Dyn.* **25** 157–82
- [16] Darmanyan S, Kobayakov A and Lederer F 1998 *JETP* **86** 682–6
- [17] Kivshar Yu S, Królikowski W and Chubykalo O A 1994 *Phys. Rev. E* **50** 5020–32
- [18] Johansson M, Aubry S, Gaididei Yu B, Christiansen P L and Rasmussen K Ø 1998 *Physica D* **119** 115–24
- [19] Howard J E and MacKay R S 1987 *J. Math. Phys.* **28** 1036–51
- [20] Kivshar Yu S and Peyrard M 1992 *Phys. Rev. A* **46** 3198–205
Daumont I, Dauxois T and Peyrard M 1997 *Nonlinearity* **10** 617–30
- [21] Carr J and Eilbeck J C 1985 *Phys. Lett.* **109A** 201–4
- [22] Eilbeck J C, Lomdahl P S and Scott A C 1985 *Physica* **16D** 318–38
- [23] MacKay R S 1986 *Nonlinear Phenomena and Chaos* ed S Sarkar (Bristol: Adam Hilger) pp 254–70
(reprinted in 1987 *Hamiltonian Dynamical Systems* ed R S MacKay and J D Meiss (Bristol: Adam Hilger) pp 137–153)
- [24] Bridges T J 1990 *Math. Proc. Camb. Phil. Soc.* **108** 575–601
- [25] Bridges T J 1991 *Math. Proc. Camb. Phil. Soc.* **109** 375–403
- [26] van der Meer J-C 1985 *The Hamiltonian Hopf Bifurcation* (Berlin: Springer)
- [27] Lahiri A and Roy M S 2001 *International Journal of Non-Linear Mechanics* **36** 787–802
- [28] Bambusi D and Vella D 2002 *Disc. Cont. Dyn. Syst. -B* **2** 389–99
- [29] De Filippo S, Fusco Girard M and Salerno M 1989 *Nonlinearity* **2** 477–87
- [30] Cruzeiro-Hansson L, Feddersen H, Flesch R, Christiansen P L, Salerno M and Scott A C 1990 *Phys. Rev. B* **42** 522–26
- [31] Hennig D 1992 *J. Phys. A: Math. Gen.* **25** 1247–57
Hennig D, Gabriel H, Jørgensen M F, Christiansen P L and Clausen C B 1995 *Phys. Rev. E* **51** 2870–6
- [32] Andersen J D and Kenkre V M 1993 *Phys. Rev. B* **47** 11 134–42
Andersen J D and Kenkre V M 1993 *Phys. Status Solidi (b)* **177** 397–404
- [33] Molina M I and Tsironis G P 1993 *Physica D* **65** 267–73.
- [34] Nemoto K, Holmes C A, Milburn G J and Munro W J 2001 *Phys. Rev. A* **63** 013604-1–6
- [35] Franzosi R and Penna V 2001 *Phys. Rev. A* **65** 013601-1–5
Franzosi R and Penna V 2002 *Laser Physics* **12** 71–6
- [36] Kevrekidis P G, Rasmussen K Ø and Bishop A R 2001 *Int. J. Mod. Phys. B* **15** 2833–900
- [37] Eilbeck J C and Johansson M 2002 The Discrete Nonlinear Schrödinger Equation – 20 Years on
Preprint nlin.PS/0211049
- [38] Christodoulides D N and Joseph R I 1988 *Opt. Lett.* **13** 794–6
- [39] Eisenberg H S, Silberberg Y, Morandotti R, Boyd A R and Aitchison J S 1998 *Phys. Rev. Lett.* **81** 3383–6
Morandotti R, Peschel U, Aitchison J S, Eisenberg H S and Silberberg Y 1999 *Phys. Rev. Lett.* **83** 2726–9
- [40] Smerzi A, Fantoni S, Giovanazzi S and Shenoy S R 1997 *Phys. Rev. Lett.* **79** 4950–3
Trombettoni A and Smerzi A 2001 *Phys. Rev. Lett.* **86** 2353–6
- [41] Abdullaev F Kh, Baizakov B B, Darmanyan S A, Konotop V V and Salerno M 2001 *Phys. Rev. A* **64** 043606-1–10
- [42] Arnol'd V I and Sevryuk M B 1986 *Nonlinear Phenomena in Plasma Physics and Hydrodynamics* ed R Z Sagdeev (Moscow: Mir) pp 31–64
Sevryuk M B 1986 *Reversible Systems* (Berlin: Springer) Chapter 6
- [43] Franzosi R and Penna V 2002 Collective modes, chaotic behavior and self-trapping in the dynamics of three coupled Bose-Einstein condensates *Preprint cond-mat/0203509*

- [44] Eilbeck J C 1987 *Physics of Many-Particle Systems* **12** ed A Davydov pp 41–51
Eilbeck J C and Scott A C 1989 *Structure, Coherence and Chaos in Dynamical Systems* ed P L Christiansen and R D Parmentier (Manchester: Manchester University Press) pp 139–59
- [45] Bridges T J 1997 *Proc. R. Soc. Lond. A* **453** 1365–95
- [46] Johansson M and Aubry S 2000 *Phys. Rev. E* **61** 5864–79
- [47] Laedke E W, Spatschek K H and Turitsyn S 1994 *Phys. Rev. Lett.* **73** 1055–9
Laedke E W, Kluth O and Spatschek K H 1996 *Phys. Rev. E* **54** 4299–311
- [48] Morgante A M, Johansson M, Aubry S and Kopidakis G 2002 *J. Phys. A: Math. Gen.* **35** 4999–5021
- [49] Feddersen H, Christiansen P L and Salerno M 1991 *Physica Scripta* **43** 353–5
- [50] Hennig D and Gabriel H 1995 *J. Phys. A: Math. Gen.* **28** 3749–56
- [51] Aubry S 1978 *Solitons and Condensed Matter Physics* ed A R Bishop and T Schneider (Berlin: Springer) pp 264–78